

POLITECNICO DI TORINO

Collegio di Ingegneria Chimica e dei Materiali

**Master of Science Course
in Materials Engineering**

Master of Science Thesis

**Fatigue behavior of Al-Si hypoeutectic
alloys: effect of processing path (SLM or
casting) and surface finishing**



Tutor/s

Prof. Claudio Francesco Badini

Dott.ssa Elisa Padovano

Sig. Stefano Plano

Candidate

Federico Minchiante

July 2019

Introduction	5
1. Additive Manufacturing	9
1.1 Introduction	9
1.2 Process chain	9
1.3 Advantages and Disadvantages	13
1.4 AM Technologies	15
1.4.1 Sheet Lamination	16
1.4.2 Binder Jetting	17
1.4.3 Direct Energy Deposition	18
1.5 Powder Bed Fusion Processes	19
1.5.1 Materials	20
1.5.2 Process Parameters	21
1.5.3 Powder Recycling	24
1.6 Automotive Applications	24
2. Aluminum alloys	27
2.1 Introduction	27
2.2 Aluminum alloys and their properties	27
2.3 casting alloys	30
2.4 Heat treatments for Al alloys	31
2.5 Fatigue behavior of Al-Si-Mg alloy	33
2.6 Surface Treatments of SLM components	36
2.6.1 Abrasive blasting	37
2.6.2 Shot-peening	37
2.6.3 Tumbling	38
2.7 Al alloys for automotive applications	39
3. Materials and Method	43
3.1 SLM process	43
3.2 Powders	45
3.3 Samples	45
3.4 Heat Treatments	47
3.5 Samples preparation	48
3.5.1 Cutting Machine	48
3.5.2 Polishing Machine	48

3.5.3 Chemical Etching	49
3.6 Optical Metallographic Microscope	49
3.7 FESEM (Field Emission Scanning Electron Microscope)	50
3.8 XRD (X-ray Diffraction)	53
3.9 Hydrostatic Scale	55
3.10 Brinell Hardness	56
3.11 Plane Bending Fatigue test	57
3.11.1 Staircase method	58
3.12 Profilometer	60
3.13 Tensile test	61
4. Experimental results	65
4.1 Microstructure and chemical composition of Al-Si-Mg alloys	65
4.2 Physical Properties	71
4.3 Mechanical properties	73
4.4 Fatigue behavior	76
4.5 Fracture surface	81
5. Conclusions	87
6. Bibliography	89

Introduction

The main target of this thesis is to investigate the differences in term of fatigue behavior between traditional manufacturing techniques, such as casting, and innovative processing methods such as additive manufacturing. The latter is a relatively young forming technology. Its history began in the early eighties, with the first studies using a thermoset polymeric material, which was the simplest material to quickly solidify by curing with UV. Initially developed as rapid prototyping mean, extensive researches of scientific community quickly convert it into an innovative way to produce near-net-shape components. The main advantages of additive manufacturing are the absolute freedom in design, the better efficiency in material usage and the relatively low energy consumption. On the contrast, the major disadvantages are linked to higher costs (both in term of material and equipment) and longer machine time compared to traditional methods. In the automotive industry, downsizing and weight reduction are key factors to meet the recent and stringent legislation for reducing fuel consumption and vehicle gas emissions. In this context, saving weight is fundamental. Using lightweight alloys, such as aluminum ones, and hollow design is the main strategy. Additive Manufacturing can be the answer to these demands because of it allows the processing of complex and trabecular geometry, as shown in fig. 1.1, starting from traditional lightweight casting alloys such as AlSi10Mg.



Fig 1.1 An example of trabecular geometry adapted to an automotive component, courtesy of GM

AlSi10Mg is a typical Al alloy used in casting processes; its near eutectic composition guarantees better castability and reduces the solidification range of temperature. This alloy can be heat treated and the presence of magnesium allows the formation of Mg₂Si hardening phase during ageing. Additively manufactured components show better mechanical properties than their casted counterparts[1], this is due to higher cooling rates of the process that produce a finer microstructure.

Since AM is becoming more and more used in the automotive world, not only for prototyping, but also for creating complete components it is very important to investigate their mechanical properties to understand if they can withstand the same stresses as their traditional manufactured counterparts. The main focus in this case is fatigue resistance to evaluate the long term use of AM components.

"Fatigue is a form of failure that occurs in structures subjected to dynamic and fluctuating stresses. Under these circumstances, it is possible for failure to occur at a stress level considerably lower than the tensile yield strength for a static load." [2]

Fatigue is the most common failure in metallic materials; it is estimated to represents about 90% of all failures in metals. There are three distinct steps in fatigue failures:

- crack initiation, where the defects in the material can act as a stress concentration point and cracks begin to form
- crack propagation, during which the crack advances with increasing number of load cycle
- final failure where the remaining section cannot withstand the applied load and catastrophically fails.

A typical fatigue surface fracture is shown in fig. 1.2. Fatigue resistance increases with the mechanical strength of the material [2], however the presence of a defect on the material surface can act as a nucleation site, reducing the fatigue resistance.

In conclusion, SLM is going to provide materials with high mechanical performance due to its fine microstructure but, on the other hand, this processing method produces components with poor surface finishing and this promotes the formation of crack and reduce fatigue life. On the base of these considerations, subsequent surface treatment is necessary. This thesis, born from a joint venture of Politecnico di Torino and Centro Ricerche Fiat, is going to compare the fatigue behavior of two materials with similar compositions produced with different technologies: AlSi7Mg cast structural components and AlSi10Mg samples produced using additive manufacturing SLM technique. Moreover the effect of surface finishing on fatigue resistance was evaluated: the fatigue behavior of AlSi10Mg samples before and after tumbling was compared to AlSi7Mg machined samples. The AlSi10Mg samples were produced by FCA prototype department while the AlSi7Mg were courtesy of

CRF. Both the materials underwent T6 heat treatments: the solubilization and quenching were carried out at Politecnico while the ageing were performed at CRF. Plane fatigue bending tests were carried out by CRF with a vibrophore; after failure, representative samples were selected according to their fatigue behavior. These were characterized in Politecnico's laboratories using a metallographic microscope, a stereomicroscope and a FESEM to investigate the microstructure and the fracture surface. This thesis is organized into 4 chapters. The first one will be an excursus of Additive manufacturing technologies with a special focus on SLM and SLM of aluminium alloys. The second chapter discuss the fatigue behavior of aluminium alloys and ways to improve it. The third one describes the processing of samples and their characterization, while the fourth and the final chapter report the obtained experimental results and discuss them.



Fig 1.2 A fatigue fracture on a AM specimen

1. Additive Manufacturing

1.1 Introduction

The term Additive manufacturing is becoming more and more used recently, but what it is AM?

According to Gibson et al. [1]"Additive manufacturing is the formalized term for what used to be called rapid prototyping and what is popularly called 3D Printing".

Rapid prototyping is in fact a way to create something quickly, without the necessity of expensive moulds or machinery, before the final release. It is used to test ideas by the developing teams or to give something tangible to clients, that can provide an immediate feedback of the product.

AM technology, that was initially developed for prototyping, is now much more capable, and it is used for many other purposes.

Given that, the term rapid prototyping is no more adequate to describe the variety of the many applications of this technology. What started as a way to produce a maquette to only give an idea of the final product, has become so much closer to the final product. To the point that some components may be directly manufactured with this technology. That is why the term Additive Manufacturing is used, with the use of Additive in comparison to Subtractive traditional technologies such as milling, lathing or machining in general.

1.2 Process chain

This paragraph will analyze the steps required to create a physical object using additive manufacturing processes.

The process chain generally requires six steps to achieve the final component, starting from just a concept.

- Generation of CAD model of the design;
- Conversion of CAD model into AM machine acceptable format;
- CAD model preparation;
- Machine setup;
- Part removal;

- Post-processing.[1]

The first step consists of imagine and design a component. A hand-drawn sketch can be the starting point or just a mere description of the product.

Then it is digitalized using CAD (computer-aided design) software, that creates a 3D model containing all the information about geometry, properties and material.

To create this tridimensional representation, reverse engineering equipment like optical or laser scanning can also be used.

When the 3D CAD model is created, the AM process chain can start. It is usually an iterative process where modifications to the CAD model are made to consider feedback from each step of the chain. When using metal powder bed technologies, crucial feedback is given by the part orientation and geometry that could influence its property anisotropy or warping.

This kind of issues may arise in the AM process and need to be addressed with revisions and design changes. Just like the “design for manufacturability” is needed in conventional manufacturing, "design for additive manufacturing" is crucial and is advancing with the technologies.

The second step is the conversion of the 3D model into a format readable for AM machinery. Essentially, all the AM technologies work with the STL (STereoLithography) file format. In the STL file, the 3D CAD model is transformed converting all the surfaces in a combination of triangles of various sizes as shown in fig 2.1.



Fig 2.1 A CAD model on the left converted into STL format on the right. [2]

AM pre-process programs combine the coordinates of the vertices and the vectors perpendicular to each triangle to determine the spatial locations of surfaces and the interior side of the component.

The STL format shows also some limitations, due to the fact that only geometry information is collected, other information contained in a CAD file such as unit, color, material, etc is eliminated. These details can be critical for the functionality of the build and their loss can cause limitations on the finished component.

To overcome this problem, the AMF (Additive Manufacturing File) format was developed, and now it is the ASTM/ISO standard format. It still stores information about geometry but it can also include dimensions, color, material, and if needed, additional information. The actual use of this additional information, such as color or material is still restricted because of the current technology in AM systems that cannot provide maximum freedom in manufacturing.

The third step is the preparation of the CAD model. When the correct file is ready, there is still a series of steps required for it to be suitable for an AM building process. The starting point is repairing the errors in the file, such as gaps between surface triangle sides or inverted perpendicular vectors, that make the program recognize the exterior as interior. After that, the machine needs a proper orientation of the 3D model made accordingly to the building platform. The information used in this step is: orientation, geometry and density. The support structures are designed to help the build of overhang or complex parts that cannot sustain themselves. Following the creation of the final design, the fundamental slicing of the model into layers of the requested height is necessary.

Then a “unit area” is determined; it represents the tiniest amount of material attainable. This, coupled with a set of strategies, is used to fill the area circumscribed by the surface of each layer.

Now, the surface information that was in the file has been processed and the machine has precise information to begin the construction of the actual component layer by layer.

The fourth step is the *machine preparation*. This can be divided into two tasks: machine hardware setup, and process control. Hardware setup involves: cleaning of the chamber, loading the powder material and a final routine check of all critical elements such as build settings, gas pressure, flow rate, oxygen sensors, etc.

The tasks in the process control are: importing and positioning of build parts in the area defined by the build plate and defining the parameters for build process, material and component.

Examples of build process parameters are: gas injection processes, material recoater motions and ventilation processes. Material parameters control powder dosing and chamber environment.

Chamber environment is regulated using inert gases such as nitrogen or argon. Oxygen concentration inside the chamber is usually kept low due to his crucial importance to the build process and quality. Typical oxygen concentration is beneath 1–2%.

Upper and lower limits of concentrations of gases are set and above these threshold values, the process will be shut down automatically. When using reactive material (such as

aluminum or titanium) in powder bed processes, the oxygen content is especially important due to safety reasons. So the inert gas flux is maintained even after the end of the process.

Component parameters are assigned to each piece and are necessary for the slicing process. When the part parameters are eventually selected the build process begins and can be controlled and monitored by the AM system itself with some feedback and built-in monitoring systems. Current systems are equipped with in-process diagnostics. A typical one is melt-pool monitoring. It emits a beam coaxial to the process beam and monitors the intensity of emission of thermal radiation from the melt-pool. In doing this, it analyzes the melt-pool dimension and the radiation intensity distribution. Another kind of in-process feedback tool is linked to the powder re-coating process. This tool takes a photograph of each layer and uses the reflectivity data obtained to determine if the layer is completely covered with powder. This analysis is used to interrupt the process and avoid the failure of builds due to inadequate coating or over-heating.

There can be a quality index extracted from these results to provide an indication of part quality.

The fifth step is the *part removal*. When the process is concluded, the manufactured component has to be taken out of the building chamber.

The build time of powder bed processes varies depending on several factors. The main one is the height of the build, which has the greatest impact on total time. The average temporal range can vary from minutes to days to weeks depending on the size and complexity of the component.

The removal process ordinarily involves raising the platform and eliminating non-sintered powder simultaneously.

Loose powder can be recycled after the process, but it needs to be treated in order to remove contaminants and undesired particulates or agglomerates. After the end of the removal step, the build is ready for post-processing. The built parts in metal powder bed AM are welded onto the build plate by support structures. The removal typically involves cutting tools such as band saws, or wire EDM (Electrical Discharge Machining).

The sixth and final step is the *post-processing*. The post-processing can vary in a broad range, depending on the AM technology used, the purpose and the requirements of the component. This can range between no post-processing to numerous supplementary steps of processing. These operations are needed to improve the surface and/or material properties of the components. AM parts have unique surface peculiarities like partially melted particles bound to the surfaces or weld-lines rastering the melt-pool in different directions. These characteristics result in a distinct surface finishing that is different from any other manufacturing processes. In metal powder bed technology, the least processing needed is

the cutting of both the component from the build plate, and the support structures from the built part. The cutting of support structures can be performed manually or can employ CNC (Computer Numerical Control) tools to also achieve the desired surface finishing and dimensional tolerances.

A typical issue in metal powder bed AM systems is the introduction of large thermal stresses into the finished part. Because of this phenomenon, the supports keep the structure in place to avoid warping. If the supports were removed before annealing, warpage in the part may occur.

Since built parts from AM frequently present porosity a suitable post-process could be HIP (Hot Isostatic Pressing). During HIP the part is put in a collapsible vessel and exposed to elevated temperature and isostatic pressure to achieve theoretical density. After being processed by HIP, the final bulk density can reach more than 95% of the true density of the material. Under these severe conditions of pressure (up to 300 MPa) and temperature (50% of melting temperature), the material undergoes localized plastic deformation and the processes of creep and solid-state diffusion bonding. This permits the needed shaping and mass transport around defects to recover them thus increasing the bulk density of the material.

Other post-processing technologies include heat treatments to improve the tensile properties in heat treatable materials and shot-peening or sand blasting or tumbling to improve the surface finishing in applications where fatigue life is crucial. These treatments were the one used in the realization of the specimens used in this thesis. The heat treatment used was a solubilization at 550° C followed by water quenching and then artificial ageing at 180° C. This treatment was chosen to homogenize the microstructure of the material and to increase its mechanical properties due to the precipitation of hardening phases.

AM technologies produce pieces with very poor surface finishing, so surface treatments are very important to increase the properties related to the surface of the material. In shot-peening and sand blasting small abrasive particles are blown on the component by pressurised air, in the case of shot-peening they are small glass beads and in sand blasting they are, as the name suggest, sand particles. The tumbling technique consist in putting the components in a barrel with abrasive particles and lubricants, and then constantly rotate the barrel to smooth the pieces.

1.3 Advantages and Disadvantages

In addition to the study of basic principles of AM process which allow the production of a component, it is necessary to evaluate the advantages and disadvantages of this technology.

Additive manufacturing forming techniques are radically different from traditional methods like machining, forming or casting processes. The main difference between traditional and additive manufacturing processes is the forming of materials. In traditional ones, the material starts as a unique body and the process happens on the whole piece; on the other hand in additive manufacturing processes the forming of material occurs with the creation of discrete elements such as voxels, filaments, and layers, that collectively constitute the final part.

This rather different nature of AM processes generates a number of advantages over traditional processes.

For example, AM guarantees high degrees of customization with little influence on manufacturing complexity or cost, because of tools and moulds, and therefore their associated costs, are not present for AM processes. A chart is shown in fig. 2.2.

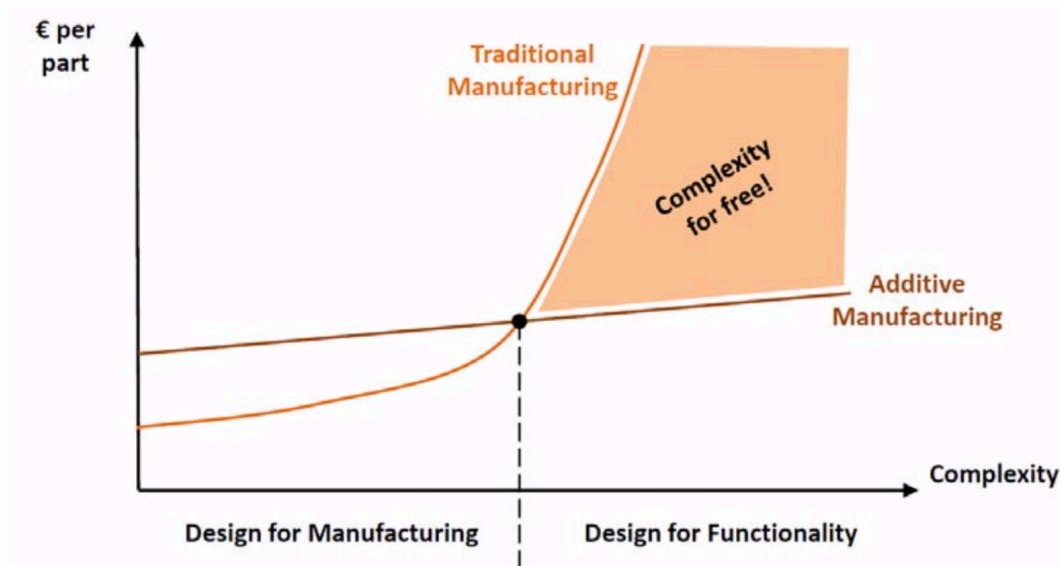


Fig 2.2 Cost comparison between additive and traditional processes. [4]

In the pilot run or in low volume production, AM shows its best features since it does not require expensive dedicated moulds and it reduces material waste saving money, time and resources.

Ultimately, AM can produce geometrically complex and compositionally heterogeneous parts while achieving the same results with traditional manufacturing can be financially prohibitive or even impossible.

The unique advantages of AM technologies encourage innovation as it drastically reduces the time required for prototyping and massively decrease the threshold for small volume production.

Additive Manufacturing processes do not present the restrictions of traditional techniques. This may enable brand-new concepts such as 3D faxing, cloud-based manufacturing, and on-demand end-user location manufacturing.[3]

Unfortunately, there are also disadvantages linked with AM processes. The main ones are: relatively small size of realized parts, limited choice in materials, high costs, poor surface finishing and anisotropy.

Starting from the first one, the dimensions of the final piece are limited by the size of the printer; typical building chambers measure 300 x 350 x 300 mm. Since it is a relatively recent technology, at the moment only a few materials have been studied on and declared fit for AM processes.

Virtually any materials can be used, but to achieve good results and properties, each material has to be tested and post-processing adjustments made subsequently.

Currently, AM is still a rather expensive technology: the cost of powders is huge compared to normal bulk material. For example, aluminium powders have an average cost of 70€/kg whereas the same material costs 3€/kg when in bulk.

Moreover, additively manufactured pieces present a rather poor surface finishing, due to the fact that loose powder tends to sinter to the surface of the part because of the high temperature of the bed and the residual heat in the material after melting. Also, rapid melting of a powder bed makes it tricky to achieve theoretical density, so a residual porosity is always present and needs to be filled with post-process treatments such as infiltration or HIP, also adding costs to the final component. [1]

Eventually, a degree of anisotropy is always present in AM components because of the growth direction, the system, in fact, works with adding layer on layer and the final structure is composed of steps.

1.4 AM Technologies

There are many existing AM technologies that can be divided into seven categories. The subsequent paragraph briefly describes each one; moreover a particular focus is dedicated to powder bed technologies.

The AM techniques which are used for the processing of metal materials can be divided on the base of the starting material and the source of energy according to the following scheme:

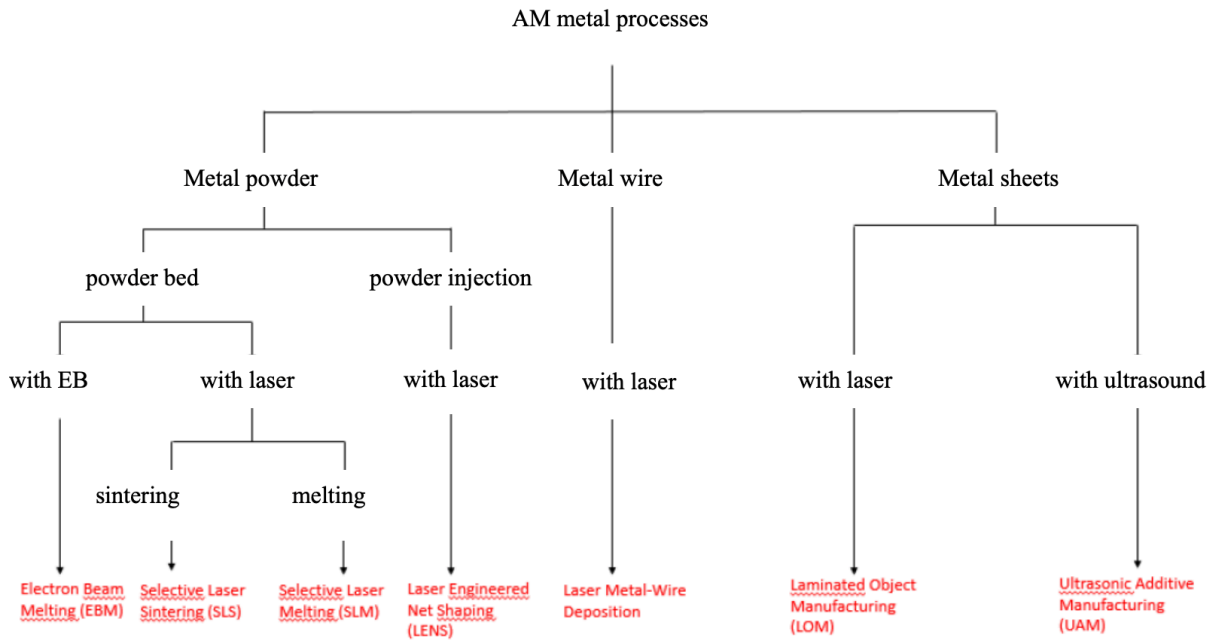


Fig. 2.3: Additive manufacturing techniques used for process metal components.

1.4.1 Sheet Lamination

This technology is also known as LOM (Laminated Object Manufacturing), it joins additive and subtractive processing to form a 3-dimensional component.

The process starts by bonding together sheets of materials such as polymers, metals, composites, etc. Then the material stack is cut and trimmed to the requested shape; laser or mechanical cut can be used. These steps are repeated layer by layer until the part is terminated. A scheme of the process is represented in fig. 2.4

Generally, the layers are joined together by heat, pressure, or aided by an adhesive.

When using metal sheets, instead of using adhesives, they can be welded together with ultrasounds.[3]

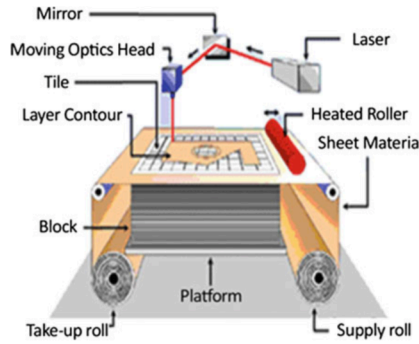


Fig 2.4 LOM Process.[3]

1.4.2 Binder Jetting

The binder jet technology is based on a blending of the powder bed process and the materials jetting process.

It starts as a PB (Powder Bed) process, so with a moving tray that goes down to create a new layer of powder with the help of a recoater. Then instead of using a source of energy that melts or sinters the particles, there is a nozzle or an array of them (like in material jetting technology) that deposit the binder to paste together the powder particles. A quick schematization is shown in fig. 2.5

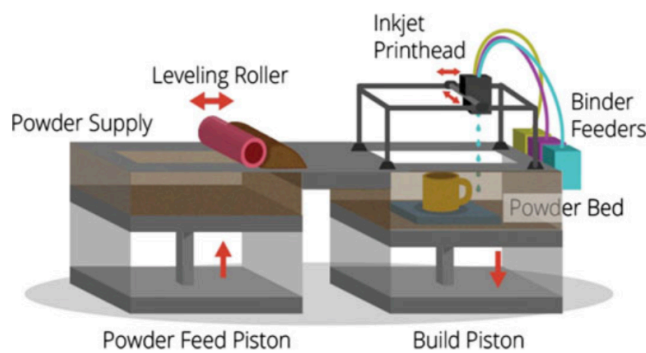


Fig 2.5 Material Jetting Process.[3]

Once the part is completed, it is surrounded by loose powder. Like in PB processes, the loose powder need to be removed.

With polymers usually, there is no need for subsequent post-processing. Nevertheless, when working with metal or ceramic, the obtained green pieces must be sintered to evaporate the binder and achieve the final mechanical properties. After sintering the component still

exhibits porosity so, if higher density is required, there can be a final treatment like HIP or infiltration. This process found application in the manufacturing of Injection Moulding dies, where steel powder is used and then infiltrated with bronze to achieve full density.[3]

1.4.3 Direct Energy Deposition

Direct Energy Deposition technology refers to the processes where raw material is directed, together with the energy input, in the desired deposition spot. Two kinds of processes are shown in fig. 2.6

The various processes differ by the form of the raw material and energy source used to join together the materials. Usually, energy sources range between laser beam, electric arc or electron beam. Feedstocks used can be powder or wire.

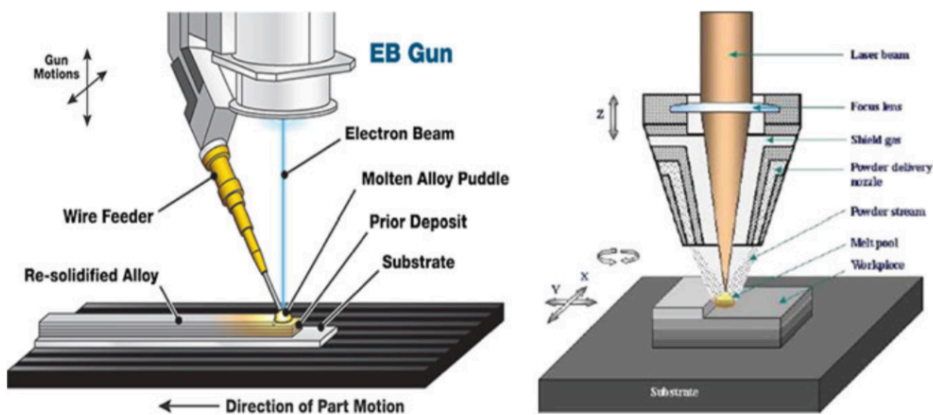


Fig 2.6 Direct Energy Deposition processes. *Right* Laser. *Left* Electron Beam.[3]

Directed energy deposition process usually leads to the formation on parts with low dimensional stability and a very rough surface finishing. To avoid this intrinsic flaw, DED is typically configured as a hybrid additive–subtractive machine. This arrangement is similar to that used in Sheet Lamination processes: the additive steps are alternate with subtractive ones, that cut the material to achieve the requested dimensions and surface finishing. Moreover, this technology requires a confined space to work, but can build very large parts. It is considered a very flexible technology that can also repair on site large mechanical or structural components.[3]

1.5 Powder Bed Fusion Processes

PBF (Powder Bed Fusion) is a family of processes that share some fundamental characteristics: one or more sources of energy to bond together powder particles, a way to restrict the fusion or sintering to a specific area in each layer, and a device to add and smooth powder layers. A common setup is shown in fig 2.7.

PBF processes are commonly used, they can use a broad range of materials (such as polymers, metals, ceramics or composites). This type of technology is becoming a mean of direct manufacturing, as the material properties are analogous to engineering-grade materials.

The three main technologies are SLM (selective laser melting), SLS (selective laser sintering) and EBM (electron beam melting). The three differs from some detail that is going to be treated in the following paragraph.

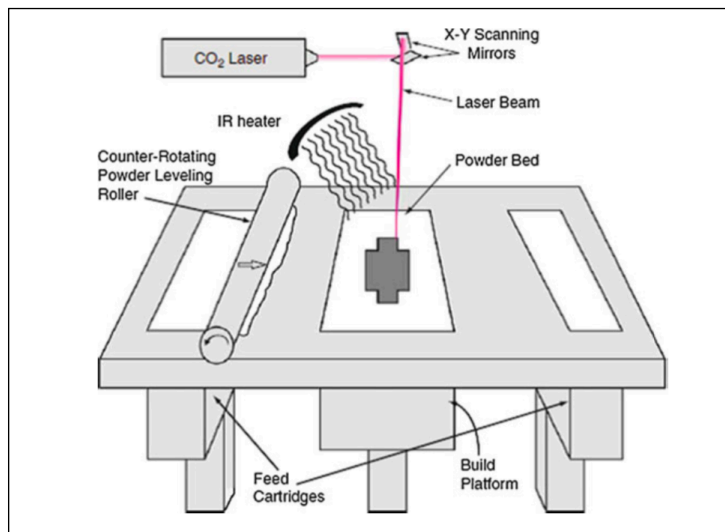


Fig 2.7 A typical PBF process scheme [3]

The first main criteria to distinguish them is the energy source. The use of lasers as energy sources for PBF has become the most widespread. The machines that use lasers are known as selective laser sintering or selective laser melting depending on the bonding technique they use. Whereas an electron beam is used as a energy source to melt metal powders in EBM machines. This latter technology requires vacuum in the building chamber to avoid obstacles in the path of electrons. This feature raises the costs of this technology since creating vacuum is more expensive than just create an inert atmosphere and also it requires more machine time to create the same piece because the air needs to be pumped off the

chamber before the job and then, after the job is done, pumped in to allow the opening of the hatch and the retrieving of the finished part. So vacuum is expensive but it allows highly reactive materials to be processed and also it can reduce porosity due to gases present in the chamber. Differently than EBM, laser manufacturing process occurs inside an enclosed chamber filled with an inert gas to avoid oxidation and thus degradation of the powder.

In all the before mentioned technologies the powder in the build platform is kept at a temperature just beneath the melting point of the material. In addition, the platform is maintained at a fixed temperature as well as the feed cartridges to preheat the reservoir of powder. The heating of powder and adjacent devices is essential to minimize the power absorption of the energy source, i.e. laser or electron beam and to limit the warping of the part due to thermal gradients.

At each step of the production process, the laser or the electron beam is focused on the bed of priorly smoothed powder and then moved creating the cross-section design. Then the building platform is lowered, the recoater deposits another layer of powder and the process can continue until the part is completed. Melting technologies such as EBM or SLM have a theoretical advantage over sintering ones like SLS because they can obtain complete fusion of the powder and thus achieve full density, this can be obtained only with perfectly tuned parameters of manufacturing.

Cooling time is required after the build ends since the piece and the loose powder are at elevated temperature and risk oxidation when exposed to an oxygen environment. Another issue can be warping of the finished part if the cooling is too rapid. After the cooling, the loose powder is removed and can begin the recycling process, and the built part can be used or it can undergo further treatments to improve properties and/or surface finishing.[1]

1.5.1 Materials

Theoretically, all materials that can be melted or sintered are suitable for PBF processes; however this thesis focuses the attention on metal components, specifically aluminum alloys, so a brief survey of metals used in PBF processes will follow. Several types of steels, titanium alloys, nickel-base alloys, aluminum alloys, cobalt-chrome alloys and eventually, powders of precious metals, such as silver and gold can be found on the market. A critical issue that needs to be considered is the formation of cracks under high cooling rates; in fact, due to the high solidification rates involving in mLS (metal Laser Sintering), cracking can occur in the built part. Another consequence of high cooling rates are the peculiar microstructures produced and subsequently, the tensile properties are distinct from those

obtained with traditional manufacturing processes. Typical metallic materials used in PBF processes are:

- Aluminum alloys: the most researched alloy is AlSi10Mg, a castable aluminum alloy, with its low melting point and low viscosity when melted is ideal for SLM technology. Other alloys include: pure aluminum, AlSi12 and AlMg.
- Titanium alloys: titanium is commonly used pure or in the Ti6Al4V alloy, since this element is highly reactive with oxygen and has an elevated melting point is difficult to cast it, AM can provide a successful way to produce components. AM technologies avoid oxygen contamination working in inert atmosphere or vacuum and can reach elevated temperature due to the focusing in a very small point of the energy source.
- Steel and iron alloys: there are quite a few types of steel used, they range from the austenitic inox 316L, to precipitation hardening alloys such as maraging 300 or 17-4 PH, to tool steel like X110CrMoVA1. With AM and the possibility to create lightweight structures, steels can now be considered even for applications where weight is a critical factor.
- Nickel alloys: most of the alloys used are superalloys for high-temperature applications such as Inconel, or Hastelloy.[6]

1.5.2 Process Parameters

The process parameters of SLM processes can be divided into four categories:

- powder-related parameters (particle shape, size, powder bed density, layer thickness, material properties)
- laser-related parameters (laser power, hatching distance, scanning speed, type of laser)
- process-related parameters (layer thickness, hatching strategy, hatch angle, growth orientation, temperature, atmosphere)

These parameters are usually heavily interdependent and they interact together. For example, the required power commonly increases as the melting point of the material increases and the powder bed temperature decreases. It is also related to the absorbance of the powder bed, that depends on factors such as material, powder shape, dimensions of particles, and packing density. Now a brief description will follow of each parameter and how it can interact with the build and the other variables in the process.

Powder Parameters

The main properties for the powders are dimensions, morphology and roughness. These affect the way the powder behave during the process. The main goals are to achieve the best packing capabilities and maximum flowability, this of course is a compromise between the parameters before mentioned. Packing increases with irregular morphology and smaller particles whereas flowability is better with larger and smoother particles. With better flowability and packing comes a better homogeneity in the layer and this means better absorbance of the laser and less residual porosity. Other powder properties come from the selected material and are: absorbance, wettability and viscosity of the molten metal.

Absorbance is defined by the ratio of radiation absorbed and radiation emitted, it depends on the material itself but also from other parameters. For example his surface, the rougher the higher the absorbance, or the packing of the layer, because the laser is lost in the voids between the particles.

Wettability is critical because it guarantees the adhesion of the fused powder to the solidified substrate, the contact angle is reduced by the presence of oxides, that is why the build is commonly conducted in a protective atmosphere. Also viscosity of the fluid act like the wettability allowing the fused particles to flow easily and better fill the porosity.

Laser Parameters

The main properties are: laser power, scanning speed and hatching distance. These three are deeply interconnected since they have to work in synergy to obtain the best results. In fact those parameters together determine the energy that is transferred to the powder bed, for example high power laser can be paired with higher speed and distance while low power laser need slower scanning and closer hatching distance. If the power transferred to the powder is excessive, too much material is melted and results in holes in the final part whereas if the power is not enough some powder will not melt causing delamination and porosity.

The two most common laser used in SLM applications are CO₂ and Nd:YAG. The CO₂ laser is cheap, reliable and efficient for this characteristics is widely diffused. It emits in the infrared spectrum whereas the Nd:YAG emits in the near infrared spectrum. Metal powder increases their absorbance with lower wavelengths, so Nd:YAG have an advantage. Also they can be directed with optical fibers and require less maintenance, all these properties results in growing adoption of this kind of laser.

Build Parameters

During the building process there several key factors that can change the final result, these include layer thickness, hatching strategy, hatch angle, growth orientation, temperature and atmosphere.

Increasing the layer thickness results in a faster process overall, however it reduces the quality of the build and also requires more laser power or slower scanning to fuse the additional powder. The dimensional accuracy is based on the layer thickness since the smallest detail must have a size larger than the thickness or they will disappear in the final build.

Hatching strategy is used to uniform the thermal stresses, this is achieved by scanning various zones of the cross-section in random or non-consecutive order. In extreme cases a pre-sinter scan is used to preheat the layer of powder with the laser and then only with the second scan the particles are melted.

The hatch angle is the angle between the directions of scanning of two consecutive layers. The variation of this angle causes variation in the material density, surface finishing and mechanical properties. Using the hatch angle is possible to define a parameter N where N is the number of consecutive layers needed to have the same scanning direction of the first, for example an angle of 120° means that 3 layers are needed so N=3. It has been observed that increasing N increases also the isotropy and the mechanical performances of the final component.

The growth direction can also influence the mechanical properties of the build since it influence the microstructure and the anisotropy of the part. Ideally to achieve better building speed the preferred growth direction is the one with the minimum height. But the adhesion of same-layer particles is better in comparison with interlayer particles so this effect must be taken in account when designing a piece.

The atmosphere in the building chamber is critical since as already mentioned the creation of oxides reduces wettability and with that the quality of the build. Also metal in powder form are more reactive since the specific surface is maximized.

Eventually the temperature of the powder bed and powder reservoirs is kept very close to the melting point because it reduces thermal stresses and warping, but also the laser needs less energy to melt the powders.

1.5.3 Powder Recycling

As already discussed in the previous paragraphs, the elevated temperature present in the building chamber can cause the sintering and agglomeration of the powder. In addition, the same elevated temperatures, when paired with reacting atmospheres, will also alter the chemical composition of the powder particles. These combined effects cause degradation of the powder even though it is not melted in the process. For some materials, these effects are negligible and thus are considered highly recyclable or infinitely recyclable. But for other materials these effects are critical, and thus recycling methodology became crucial when trying to reuse the powders in subsequent builds. Used powders are commonly selected before mixing with virgin ones. The main particles sorting methods are based on the use of a vibratory sieving device or an air classifier. Air classifiers can be more efficient than sieving because they blend the particles together and they can also divide agglomerates. These characteristics help to recycle a larger fraction of material. However, air classifiers are more complex and above all more expensive than sieving systems. Whichever the sorting method used is, it is very important that the new and used powders are well-mixed; otherwise, when building new parts there is the risk to have different properties in different zones of the component.[2]

1.6 Automotive Applications

The automotive industry was one of the first users of AM processes. They pioneered different applications of these techniques in the product development. Starting from rapid prototyping to help the design compartment, AM is nowadays addressed to actual manufacturing of structural components in high-end applications such as luxury or motorsports. In addition to these uses, AM processes are used to test the assembly lines and operations to spot potential issues, before production assembly actually commences. Since in the automotive world a change in the production line involves large investments, the ability to foresee problems in production step resulted in considerable savings. For custom-made cars or low-volume production, AM can actually be a cheap solution for some parts. These applications range from custom parts on high-end luxury cars or replacement parts on antique cars, where reactivating the old productive line could be too expensive to justify the production of small lots of components. In the luxury cars sector, there is the example of Bentley Motors which used to manufacture some custom interior components, such as bezels, that were subsequently covered in leather and other materials to accommodate the requests of the customer.

For motorsports applications, Formula 1 has been a leader in adopting AM technologies. They started using AM for rapid prototyping, but after understating the potential of 3d printing, some of the teams started mounting AM parts on their single-seaters as early as the mid-2000s. In the beginning, the parts were typically nonstructural polymer PBF parts, but with the recent advancements of metal technologies, similarly to the aerospace industry, the teams started to adopt additively manufactured components in engines and structural compartment shown in fig. 2.8 and 2.9 Following the F1, teams from other racing categories, including Indycar and NASCAR, started using AM processes.



Fig 2.8 Piston made by AM[5].

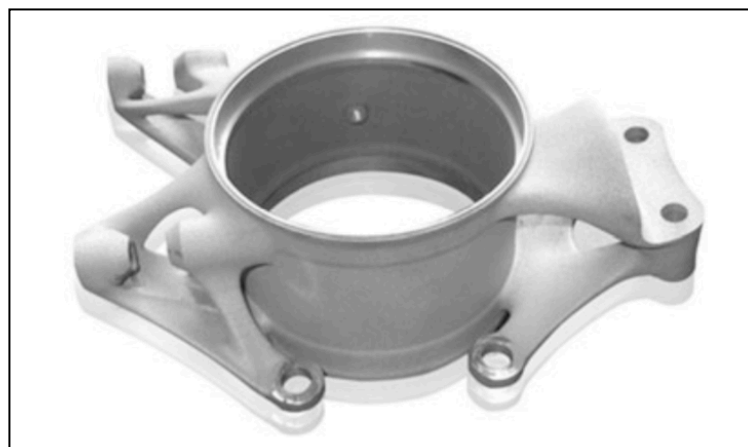


Fig 2.9 Racecar steering knuckle made by AM[5].

2. Aluminum alloys

2.1 Introduction

This chapter will investigate the characteristics of aluminum alloys and their classification in addition to the main surface processing and heat treatments which are currently used to improve the properties of this material. Moreover, because of this thesis is focused on the fatigue behavior of Al-Si components for automotive applications, a more in-depth study on these topics are reported.

2.2 Aluminum alloys and their properties

Aluminum is the third most common element in the earth's crust: with an abundance of 8% in mass is just behind oxygen and silicon. Because of its high chemical reactivity, it is very hard to find it as a lone element in a metallic state, but it is often found as a compound, combined in ores.

Both pure aluminum and aluminum alloys are characterized by a relatively low melting point, low density and good ductility. It presents a face-centered-cubic (FCC) crystal structure and a density of 2,7 g/cm³; the FCC crystal structure gives Al high ductility since it presents close-packed planes where atoms could slide smoothly. This means that, like in other metals that present the same crystal structure such as gold, copper or lead, aluminum can be easily deformed and shaped.

Aluminum is one of the first ever used lightweight alloy; thanks to its low density, it finds applications as a substitute for mechanical parts made with ferrous alloys. However, the elastic modulus of steel is three times higher than aluminum one. To achieve the same stiffness using an Al panel is therefore necessary to multiply the thickness of the steel panel by the cubic root of the ratio between the elastic moduli [7]. This means that an aluminum panel should be 1,45 times thicker than a steel one. However the density of steel (7,8 g/cm³) is much higher respect to the Al one, so even using more material, Al allows to reduce the mass component of approximately 50%.

Al and its alloys show both high thermal and electrical conductivity; moreover it has good corrosion resistance thanks to the phenomenon of passivation. In fact, because of its high affinity with oxygen, aluminum tends to create a thin surface layer of aluminum oxide, that protects the bulk material from further corrosion. Pure Al has intrinsic poor mechanical

properties, but alloying it with other elements such as silicon, copper, magnesium or lithium, it is possible to drastically improve its tensile properties while maintaining low density. For example, pure aluminum has a yield strength of 34,5 MPa [8], while modern aeronautical alloys can reach peaks up to 625 MPa [7].

Aluminum alloys are classified into two main categories: cast alloys and wrought alloys. These two macro-categories can be further classified by alloying elements with a numerical system showed in tab. 3.1.

The designation system of wrought alloy involves the use of 4 number: the first one indicates the main alloying element, the second digit, if it is different from 0, indicates a modification of the specific alloy; the third and fourth numbers are arbitrary digits, reported in order to identify a specific alloy in the series. On the other hand, the cast alloy designation system consists of 3 numbers plus a decimal one. As previously reported, the first digit represent the principal alloying element, while the second and the third ones are arbitrary numbers used to identify a specific alloy in the series. The decimal digit indicates if the alloy is a casting (=) or an ingot (.1 or .2).

Another way to categorize aluminum alloys is between age hardening alloys (they can gain strength if thermal treated) and non age hardening alloys as shown in fig.3.1 Finally the designation of the alloy requires the indication of the metallurgic state of the material using (tab 3.2) a letter to identify the kind of processing the material is submitted.

Wrought Al alloys		Cast Al alloys	
1XXX	Pure Al (99.9%)	1XX.X	Pure Al(99.9%)
2XXX	Al-Cu	2XX.X	Al-Cu
3XXX	Al-Mn	3XX.X	Al-Si-(Cu/Mg)
4XXX	Al-Si	4XX.X	Al-Si
5XXX	Al-Mg	5XX.X	Al-Mg
6XXX	Al-Mg-Si	6XX.X	Not used alloys
7XXX	Al-Zn	7XX.X	Al-Zn
8XXX	Al-Li	8XX.X	Al-Sn
		9XX.X	Others

Tab 3.1 Classification of Al alloys

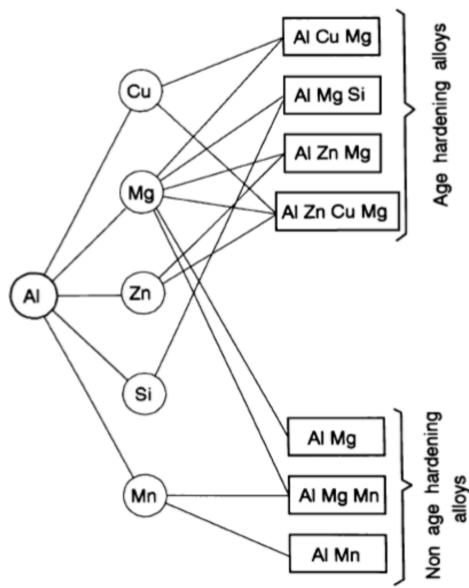


Fig 3.1 Classification of Al alloys by heat treatment

Designation	Metallurgical State
F	As fabricated
O	Annealed
H	Strain hardened
H1	Strain hardened w/o heat treatment
H2	Strain hardened and partial annealing
H3	Strain hardened and stabilized
W	Only solution heat treatment
T	Tempered

Tab 3.2 Designation of Al alloys

2.3 casting alloys

Aluminum casting alloys presents a series of benefits, above all an excellent castability. This comes from some unique characteristics such as low melting point, high fluidity, short casting cycles, a low tendency for hot cracking, a good surface finish without further steps and chemical stability.[9]

As already mentioned pure Al has a melting point of 660°C. It is often used in a eutectic or near-eutectic composition that lower the melting temperature; for example, the AlSi10Mg alloy used in this thesis melts at 577°C [10]. Al-Si phase diagram is shown in fig 3.2 with a focus on the eutectic.[11] The presence of Silicon in this family of alloys has two effects: on one side it lowers the melting temperature and on the other side, it behaves as a strengthening phase with its hard crystals. However, the presence of too much Si in the alloy involves disadvantage: Si can in fact act as inclusions, lowering the mechanical properties such as tensile strength or fatigue resistance. Hypereutectic alloys of Al and Si are commonly used when wear resistance and good performances in temperature are needed.

Al-Si alloys are the most commonly used in the automotive world and in general the most used in casting final components due to their unpaired castability.

In SLM process the properties required for the metal powders are similar to the ones needed in casting. These are: a low melting point, a short range of solidification, good wettability and high absorbance of the laser.

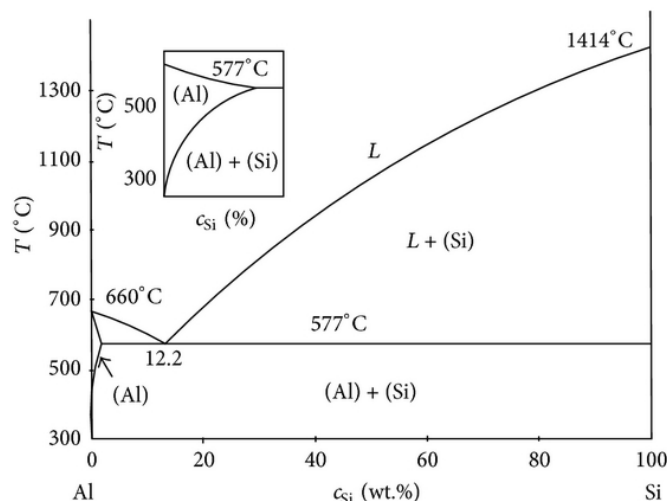


Fig 3.2 Al-Si phase diagram [11]

AlSi10Mg is a casting hypoeutectic alloy that presents these characteristics. As shown in fig. 3.2 the eutectic composition between Al and Si is at 11,7% of Si in weight at 577°C of temperature. Since it is a near eutectic alloy the melting point is minimal and has a short range of solidification. Moreover the silicon contained in the alloy improves the wettability this way the layers can adhere more easily between them making easier the SLM process. Silicon has another benefit, it increases the absorbance of the metal allowing the use of lower power lasers. Eventually, AlSi10Mg due to the presence of Si and Mg can be heat treated to achieve better performances. During ageing, these two elements precipitate creating reinforcing phases such as pure Si or the intermetallic Mg₂Si.

2.4 Heat treatments for Al alloys

Some families of aluminum alloys, as beforehand mentioned, can be heat treated to modify and enhance their properties. The designation for heat treated alloys consists of the letter T followed by a number, that indicates the kind of applied treatment, as shown in tab 3.3. If the part is simply annealed the designation is the letter O.

Annealing is used to relieve the residual stresses in the material and to achieve mechanical and thermodynamical equilibrium. It can be used in both heat treatable and non-heat-treatable alloys and it consists of three steps: heating the piece below its melting point, maintaining the temperature and ultimately slow cooling.

T1	Cooled from an elevated-temperature shaping process and naturally aged
T2	Cooled from an elevated-temperature shaping process, cold worked and naturally aged
T3	Solution heat-treated, cold worked and naturally aged
T4	Solution heat-treated and naturally aged
T5	Cooled from an elevated-temperature shaping process and artificially aged
T6	Solution heat-treated and artificially aged
T7	Solution heat-treated and overaged/stabilized
T8	Solution heat-treated, cold worked and artificially aged
T9	Solution heat-treated, artificially aged and cold worked
T10	Cooled from an elevated-temperature shaping process, cold worked and artificially aged

Tab 3.3 Aluminum alloys heat treatments

Heat treatable alloys can be strengthened when heat treated by a phenomenon called precipitation hardening. The precipitation of harder phases causes distortions in the material crystal lattice causing an increase of the tensile strength and the hardness of the alloy. This heat treatment is constituted by three steps: solution heat treatment, quench and ageing.

The solution heat-treatment is carried on at a temperature called T_s (solubilization temperature) and lasts up to few hours to allow the complete solubilization of the alloying elements. The T_s must be close to the melting point; for example, AlSi alloys that melt around 580°C , should be treated at temperatures close to 560°C .

Afterwards, the metal is quenched, usually in water. Quenching is a rapid cooling from T_s to room temperature that is used to prevent diffusive processes in the alloy and produce a supersaturated solid solution at low temperatures. Since the solution obtained is metastable, the process of ageing starts immediately after the quench. The latter can be done naturally or artificially, depending on the type of alloy that is treated. Natural ageing is performed at room temperature while artificial one requires a higher temperature, and thus the use of a furnace. These two kind of aging are associated to different microstructural changes. During the process, hard phases start precipitating in the solid solution. The first solute clusters that

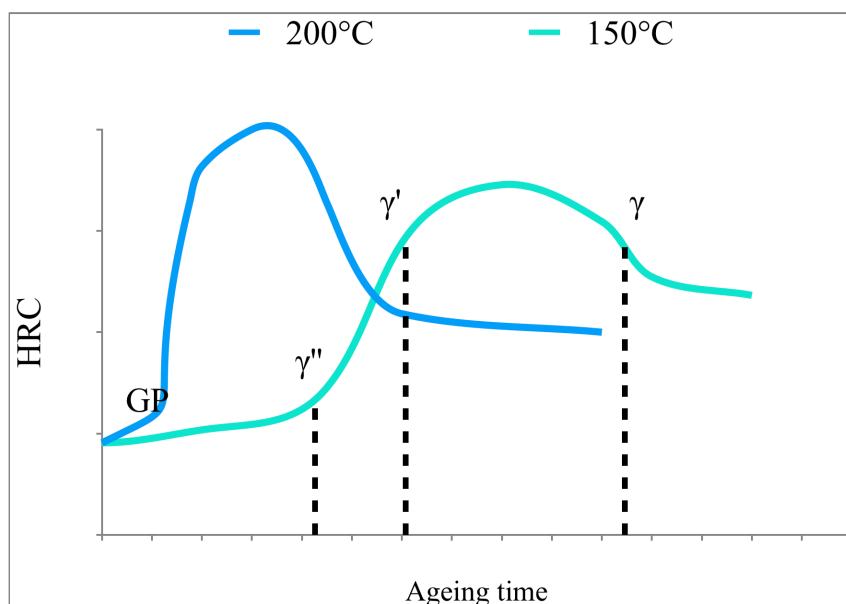


Fig 3.3 Al-Si-Mg ageing curve

nucleate are called Guinier-Preston zones; these particles are small and do not create difficulties in the movements of dislocation, thus the increase of hardness is limited.

When the aging time increases, a coherent phase γ'' starts to nucleate. Coherent means that the precipitated phase has the same crystal lattice of the matrix, in this case, FCC.

The γ'' phase is bigger than the GP zones that is why it induces more reticular distortion and more strengthening of the alloy. The γ'' phase is metastable and evolves with time in the γ' phase, which is still metastable, to the stable phase γ , that in the case of the AlSi10Mg alloy is Mg₂Si. An example of an ageing curve is shown in fig 3.3.

2.5 Fatigue behavior of Al-Si-Mg alloy

Fatigue is a form of damaging that occurs in materials under cyclic stresses; it results in material failure even though the applied stresses are well below the material tensile strength. Since the material is not a perfect crystal, repeated stresses, even if modest, target the small inclusions or defects and tend to increase them with every cycle; this leads to the initiation of the crack. After the initiation, the crack propagates with each application of stress, and this creates the typical fatigue striations on the fracture surface. Striations form because of plasticity at the crack tip. When eventually the resistant section cannot withstand the load, the part incurs in catastrophic failure. A typical fatigue failure is shown in fig 3.4, where it is possible to observe the initiation and the propagation of the crack. Failures due to fatigue are very critical and dangerous because they can happen in normal operative conditions, without excessive loads are applied and above all without notice.

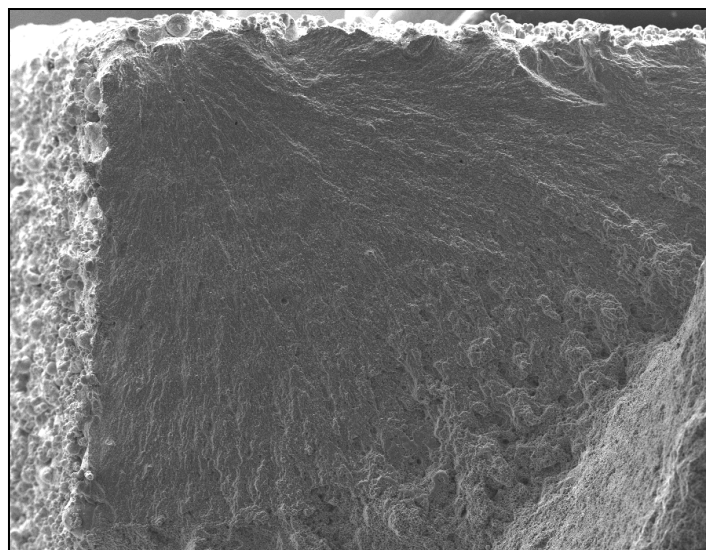


Fig 3.4 Fracture surface of a fatigue failure

As mentioned before, fatigue failure occurs in three distinct steps that can be following summarized:

- Initiation: the initiation point of the crack is usually located on or near the surface, close to defects such as porosity, inclusions, scratches, and small fillets. Even if there were no defects in the affected zone, cyclic stresses can move the dislocations inside the material; this movement creates 45° slip bands that generate notches. These notches can initiate the crack, so fatigue is an ever-present phenomenon.
- Propagation: after initiation, the crack starts to propagate inside the material, usually perpendicularly to the direction of the applied load. Propagation usually moves between the grains.[15] When the area is subjected to traction stresses the crack opens, when in compression it closes but does not recover the previous growth. This process is repeated with each cycle causing the propagation of the crack and the formation of the typical beach marks, concentric striations around the initiation point.
- Failure: during the propagation step, the material incurs in a progressive damaging that limits its ability to withstand loads. When the resistant section is reduced enough in such a way that the applied stress is equal to the material tensile strength, the component fails abruptly.

These peculiarities make the fatigue failures very hard to foresee. Since this phenomenon is mainly due to pre-existing defects in the material, it must be treated statistically because there is no way to predict the number of defects that can nucleate a crack inside each component.

To investigate the fatigue behavior of a certain material, several specimens are subjected to cycles with a maximum and a minimum stresses applied at every cycle. The results of these tests are plotted on a bilogarithmic graphic that shows the strain on the y-axis and the number of cycles on the x-axis. This curve is called a Wohler curve; it takes the name from the German engineer who started to investigate the phenomenon of fatigue in materials. Fig. 3.5 shows the comparison between two Wohler curves: it is possible to observe that steels show a real fatigue limit, where the curve has a plateau; the stress amplitude doesn't change by increasing the number of cycles. On the other hand, aluminum alloys do not have this limit and the curve continues to decrease by increasing the number of cycles. This is the reason why aluminum alloys are typically tested up to a predetermined number of cycles requested by designers, usually one million or ten million cycles depending on the application.

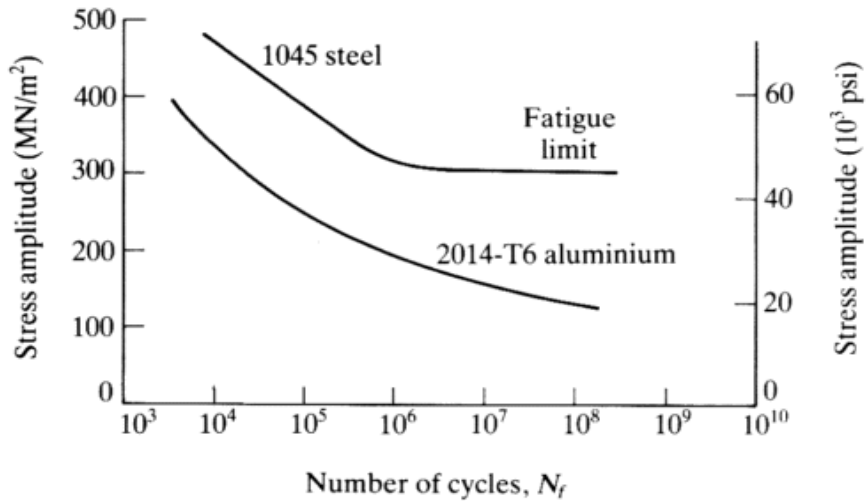


Fig 3.5 Comparison between Wohler curves [15]

The fatigue behavior in materials is influenced by many factors; the main ones are:

- Specimen size and geometry: Since fatigue is a statistical phenomenon, the size of the component is crucial. Bigger is the sample, higher is the probability to find a critical defect inside. Another critical issue in the study of fatigue is the presence of notches on the specimen; a variation of component section and shape can be linked to a project requirement. A notch is a preferential fatigue crack initiation because of it concentrates the applied stress at its tip.
- Surface finishing: This is a critical factor because of the nucleation of the crack typically starts on the surface, and defects in this area can heavily reduce fatigue resistance. The effect of a rough surface on fatigue resistance is lower for ductile materials, such as aluminum, respect to brittle ones; this is due to their ability to deform plastically decreasing the crack propagation.
- Heat or surface treatment: residual compression stresses on the surface of the material increase the fatigue resistance. This is due to the stress that favors the closure of the crack when it starts to propagate. There are several methods to develop residual surface stresses: they can be mechanics such as cold working or shot-peening, thermal like tempering, or chemical such as nitriding or cementation.
- Microstructure: the size of grains is important since the crack propagation is a transgranular phenomenon; finer grains guarantee a higher fatigue resistance as shown in fig 3.8. Moreover, the direction of the grains influences fatigue properties, resistance is in fact higher when the strain is parallel to the grains. Precipitates and inclusions should be globular and smooth to achieve the best performances. Finally, strain

hardening should be avoided because it increases the tensions and the defects inside the material promoting cracks propagation.

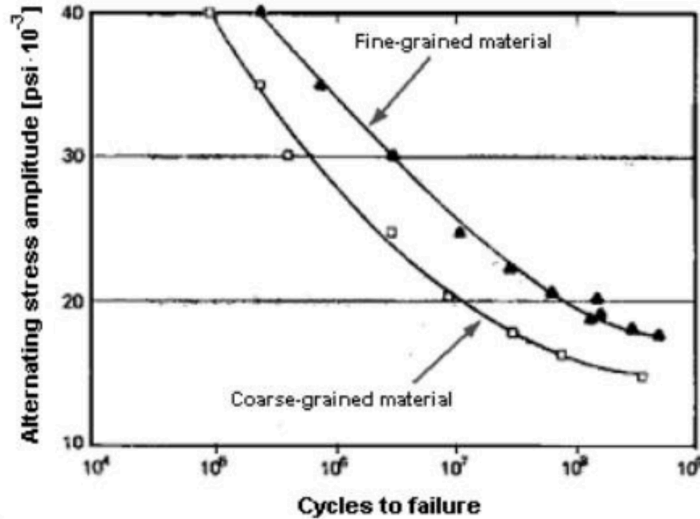


Fig 3.8 Variation of fatigue properties with grain size [16]

2.6 Surface Treatments of SLM components

The surface roughness of SLM parts in the as-built condition is one of the main drawback in adopting this technology. The main factors which influence the final roughness are the balling and dross formation in the melt pools [Calignano et] and the adhesion of partially melted particles of powder to the surface parts [Barari]. The surface finish is an important item that need to be taken into account for many applications such as those that requires good corrosion resistance or fatigue strength. Indeed, superficial roughness is one of the main cause of fatigue failure since the surface defects and irregularities act as crack nucleation sites.

Traditionally, a cast part is machined when it is necessary to further improve the surface quality. On the contrast, since one of the main advantage of AM respect to the more conventional techniques is the geometrical freedom, the post process of the components represents an extra step in the manufacturing process, which requires a higher production cost.

The following surface treatments are taken into consideration in order to improve the surface finishing and consequently improve the fatigue resistance, which is investigated in this work of thesis: abrasive blasting, shot peening and tumbling.

2.6.1 Abrasive blasting

Abrasive blasting is a process which aims to smooth and clean the surface of hard material by forcing solid particles at high speeds and under pressure across the material surface. Different kind of particles can be used such as silica particles in sandblasting and metallic or ceramic beads in shot blasting. In the case of AM parts, abrasive blasting is used to remove semi-melted powder particles from the surface improving the surface quality. This technology offers a few advantages: it is cheap since it requires only compressed air, abrasive particles, and a chamber to work in; moreover there are not limit in samples geometry, in fact it is possible to process parts with corners or crannies. Finally, there are few parameters to work with, such as fluid pressure, particle size and shape, and exposure time. On the other hand, it has some downsides: it often needs to be carried on by an operator since the cost for automatization should eliminate the economic benefits; moreover the time required linearly increases with the number of pieces to be processed, limiting it to small numbers production.

2.6.2 Shot-peening

Shot-peening is an evolution of the previous technology; it still involves particles been projected onto the surface but their properties such as the geometry and size distribution are controlled. The particles used in shot-peening of non-ferrous alloys are usually ceramic microspheres, usually made of glass. The dimensional range of these particles is carefully controlled during the process; a system in fact eliminates non-conform or broken spheres. The main goal of solid particles is to bounce onto the surface to create a dimple and, as a consequent, a state of tension in the superficial layers of the material rises as shown in fig 3.4.[12] So this treatment, in addition to cleaning the surface, also creates residual stresses and strain hardening that improves the fatigue behavior of the component. The presence of residual stresses in the surface layers tends to close the crack before it can propagate; moreover the material is hardened by cold working and slows down the initiation phase.[13]

Shot-peening allows to obtain high quality surface in the final pieces, but it shows some drawbacks: first of all every material needs different parameters to achieve the best results, so the process has to be optimized for every new material. Moreover, the particles wear faster and must be replaced often. Lastly, such as for the abrasive blasting technology, the working time increases with the number of pieces. All these characteristics made shot-peening an expensive technique.

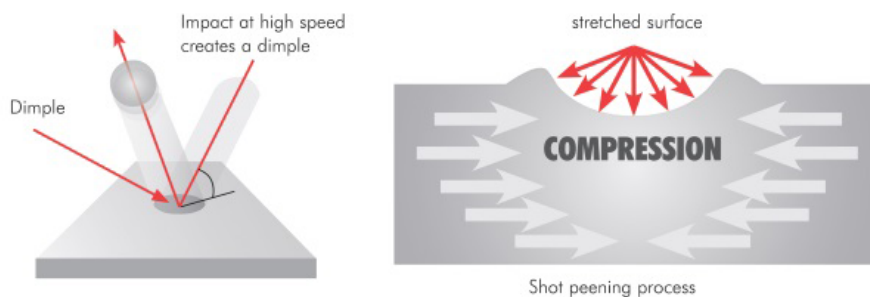


Fig 3.4 Shot-peening scheme [12]

2.6.3 Tumbling

Tumbling or vibratory machining is typically used for finishing, deburring and polishing the produced components [14]. As abrasive blasting, tumbling only cleans the surface and improves the roughness. The process is carried out in a closed tumble that contains the components to be treated, a lubricant, and the abrasive media. The latter are shown in fig 3.5. When all the components are in the tumble, it begins to slowly rotate or vibrate in order to move the inside pieces and cause the abrasion of the softer one, i.e. the metal. This technology has many applications, from polishing precious metals in the jewelry industry to rims to electronic components[14].

The big advantage of this technology is that the working time doesn't change with the number of worked pieces, so it is possible to polish numerous parts at the same time. This makes the treatment cheaper with large batches of components.



Fig 3.5 Abrasive used in tumbling

2.7 Al alloys for automotive applications

Due to their peculiar characteristics, above all low density and resistance to corrosion, Al alloys are used in a wide range of manufacturing fields. The most meaningful sectors are: aeronautical, aerospace, railway and automotive. In the latter field aluminum alloys have been used in car manufacturing for over a century; in fact it is always been a noble material in the automotive world. The traditional metal used in automotive construction is steel, but Al alloys can replace it allowing for weight reduction. In the past Al alloys were usually reserved for lightweight and particular cars. However in modern days, due to ever so strict emission and consumption laws aluminum has become more and more widespread to reduce the mass of the modern cars.

The first use of lightweight alloys in a car was in the first decades of the XX century for the manufacture of body panels; this was the first attempt to reduce the vehicle weight and use a more ductile material to allow the coach-builders to create masterpieces. In that period cars had a "rolling chassis" produced by the manufacturer and then every owner would commission a bespoke body to a coach-builder. A famous example is the Carrozzeria Touring Superleggera, established in Milan, who patented the eponymous construction technology Superleggera in 1936. This technology consisted of a structural framework of small-diameter steel tubes covered with body panels made in Duralumin.

Duralumin was one of the first age-hardenable al alloys, it used copper and magnesium as alloying elements; this material, nowadays obsolete, at the time was used in aviation and high-end automotive. The Superleggera system allowed for manufacturing flexibility and the creation of stunning and innovative body shapes. An example is shown in fig 3.9 with the beautiful Alfa Romeo 8C Mille Miglia of 1936.



Fig 3.9 Alfa Romeo 8C with aluminum body

The use of aluminum is not limited to aesthetic purposes, since at the beginning of the car history, manufacturers sensed that weight reduction was the best way to improve their vehicles, especially in motorsport. The first example of lightweight alloy in the engine compartment dates 1901[17] with the Mercedes 35 HP, shown in fig 3.10; this revolutionary racing machine featured the main bearings and the crankcase made in Magnalium, an alloy made of Al and Mg. The use of lightweight alloys in engine progressively evolved; nowadays high performance engines are almost entirely made out of aluminum alloys.

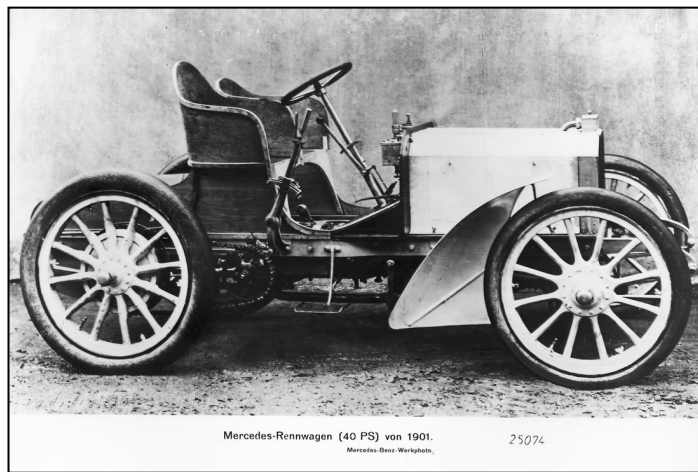


Fig 3.10 Mercedes Benz 35HP

Aluminum is also used for structural purposes, Colin Chapman firstly introduced in 1962 the first ever aluminum monocoque with the F1 racing car Lotus 25 shown in fig 3.11. The use of a monocoque made the chassis three times stiffer than the previous single-seater; moreover the use of aluminum allowed to reduce the weight by 50%. This technology arrived on the mass-produced market only in 1994 with the Audi A8 that featured the first aluminum body.



Fig 3.11 Lotus 25 of 1962

Aluminum alloys are also used in wheels, heat exchanger, bumpers, safety plates, suspensions and transmissions and also for decorative pieces inside the passenger compartment such as trimming or instrumentation. In the 1970s the average car had 35 kg of Al alloy, today it has 152 kg and projections show that for 2025 the aluminum content will reach 250 kg. [17]

3. Materials and Method

This chapter is going to illustrate the processes and tests used in this thesis to achieve the final result. Firstly, it will be described the AM process used to realize the samples, including powders and machine parameters, then the heat treatment process and successively the surface finishing process. Eventually, all the measurement instruments will be presented with a brief explanation of their operating principles.

3.1 SLM process

The samples were produced by FCA NV at the Prototypes Department located in Mirafiori Plant in Turin. The machine used was the EOS M290 produced by EOS GmbH, it is shown in fig. 4.1.



Fig. 4.1 EOS M290

This AM machine is used to manufacture metal parts starting from a CAD design. it is possible to process a wide range of material with this machine, all provided by EOS: EOS Aluminium AlSi10Mg, EOS CobaltChrome MP1, EOS MaragingSteel MS1, EOS NickelAlloy HX, EOS NickelAlloy IN625, EOS NickelAlloy IN718, EOS StainlessSteel CX, EOS StainlessSteel PH1, EOS StainlessSteel 17-4PH, EOS StainlessSteel 316L, EOS Titanium Ti64, EOS Titanium Ti64ELI, EOS Titanium TiCP Grade 2.

The building chamber of the M290 is kept in an inert atmosphere by using nitrogen or argon to avoid powder oxidation. The hatching strategy suggested by the manufacturer is a rotation of 67° between the laser tracks in each layer to avoid anisotropy.[17] A data sheet of the printer is reported in tab 4.1.

The samples were produced with the parameters shown in tab 4.2.

Building volume	250 mm x 250mm x 325 mm
Laser type	Yb-fiber laser; 400w
Precision optics	F-theta-lens; high-speed scanner
Scan speed	up to 7,0 m/s
Focus diameter	100 µm
Power supply	32 A
Power consumption	max. 8,5 kW/ typical 3,2 kW
Nitrogen generator	integrated
Compressed air supply	7000 hPa; 20m ³ /h

Tab 4.1 EOS M290 spec sheet

Parameters	Value
Hatching distance	0,19 mm
Scanning speed	1300 mm/s
Laser power	370 W
Beam offset	0,02 mm
Hatching strategy	Along X axis, with rotation of 67° layer by layer
Hatching width	7 mm
Hatching overlay	0,02 mm
Layer thickness	30 µm

Tab 4.2 EOS M290 building parameters

3.2 Powders

The samples were produced using AlSi10Mg powders produced and supplied by EOS GmbH. The powders were gas atomized and the chemical composition provided by the manufacturer is presented in fig. 4.2.

These powders are supplied in a fine state that is optimized for EOSINT machines.

Element (wt%)	Al	Si	Fe	Cu	Mn	Mg	Zn	Ti
Minum	Balance	9.00	-	-	0.20	0.20	-	-
Actual	Balance	9.70	0.20	<0.01	0.38	0.44	<0.01	0.01
Maximum	Balance	11.00	0.55	0.05	0.45	0.45	0.10	0.15

Fig 4.2 EOS AlSi10Mg powder composition

3.3 Samples

For the analysis three kinds of samples of AlSi10Mg were produced to investigate the mechanical properties of this alloy after heat treatment.

Another batch of cast T6 AlSi7Mg was used to make a comparison between traditional and AM processes.

- Plane bending fatigue: hourglass-shaped specimens with a rectangular section, see fig. 4.3 for the technical drawing. These samples were grown in the Z direction (vertical) with 30 microns of layer thickness and heat treated, successively half of these samples were tumbled to improve the surface finishing. The cast samples were machined from a solid part of aluminum in the same shape and size. These specimens were used to determine the fatigue limit of the alloy at 10 million cycles.
- Tensile strength: hourglass-shaped specimens with a round section, see fig 4.4 for the technical drawing. These samples were grown in the Z direction (vertical) and heat treated.

- Surface Treatment: To improve the surface finishing of this material a few samples in the shape of a parallelepiped were produced and heat treated. These were used in test runs of the tumbling machine to tune a suitable process for this alloy, they are shown in fig 4.5.

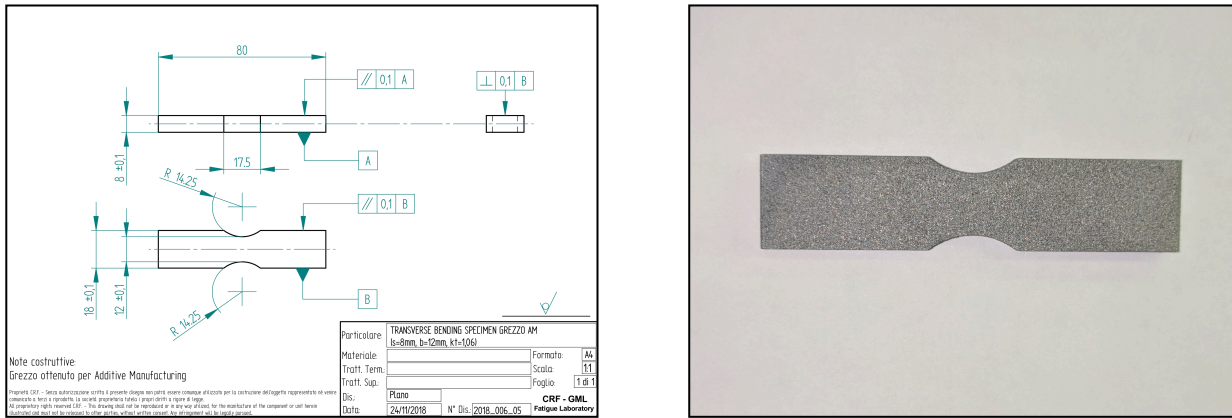


Fig 4.3 Plane bending sample, technical drawing and photo

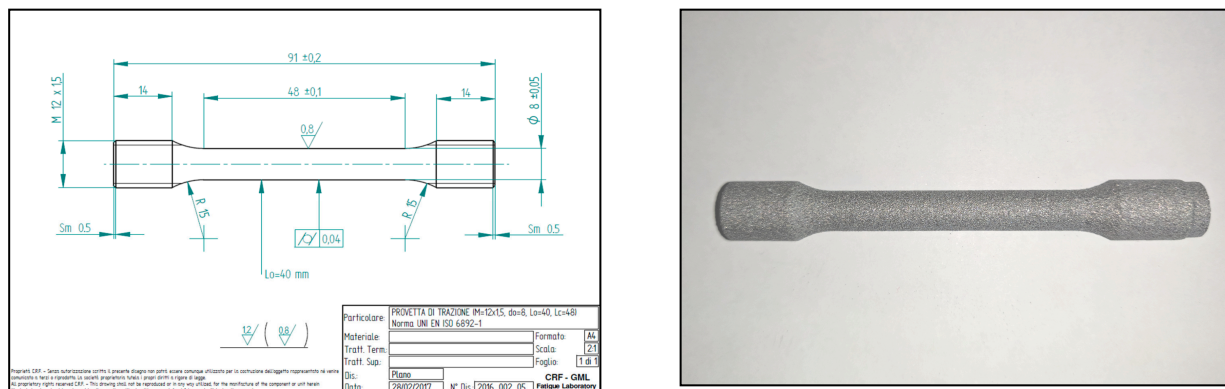


Fig 4.4 Tensile strength sample, technical drawing and photo

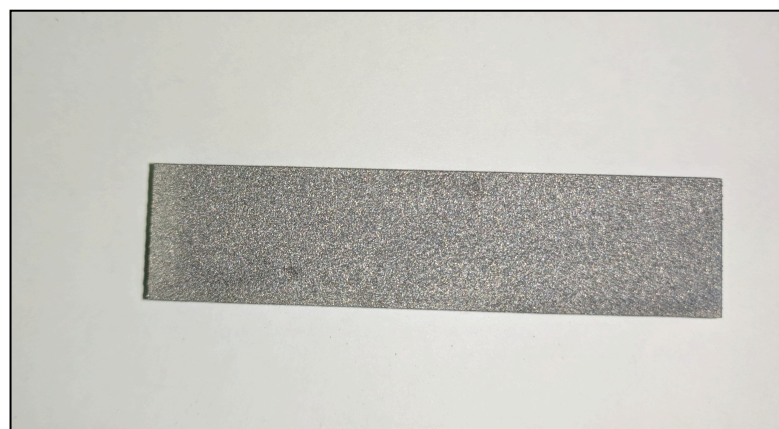


Fig 4.5 Surface treatment test sample

3.4 Heat Treatments

The main target of the heat treatment was to achieve a balance between the mechanical properties of the AlSi10Mg alloy, the process was developed in a previous work[18]. The selected heat treatment allows to optimize the tensile strength. It consists of a solubilization at 550°C for 2h followed by water quench, after that the ageing process was carried on at 180°C for 6h and then the pieces were cooled in air. The Nabertherm oven, model RHTC 80-710/15, was used for the solubilization. The calibration of the temperature has been done with a type K Inconel thermocouple.

The samples were contained in an alumina vessel in batches of 5 and inserted inside the cold oven. Successively argon was fluxed inside the chamber to avoid contamination in temperature. The oven was heated to 550°C in 2h, afterwards then the aluminium samples were kept at 550°C for 2h and then quenched. After the quench, the samples were transported to the CRF fatigue laboratory to be aged in a stove for 6h at 180°C and afterwards tested. The Nabertherm oven is shown in fig. 4.6.

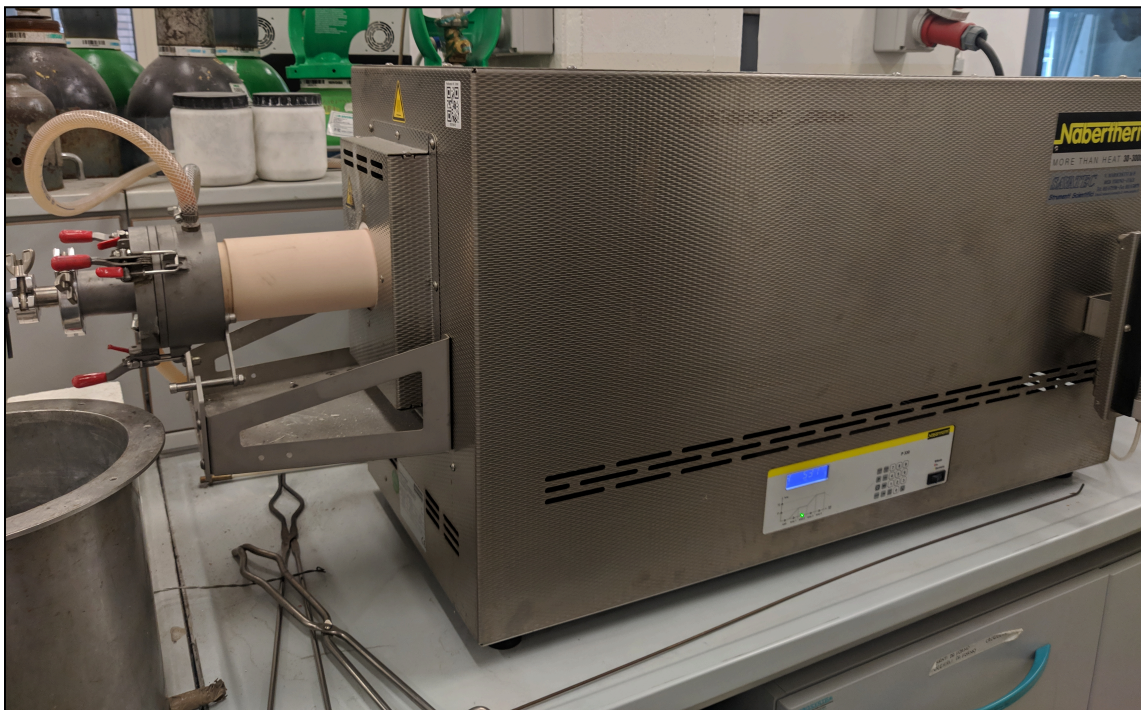


Fig 4.6 Nabertherm Oven

3.5 Samples preparation

The preparation of samples for the different characterization tests involved different steps: they were cut, cleaned and polished in order to study the microstructure with optical and electron microscopes. Furtherly, they were weighed on a hydrostatic balance to measure the density; moreover X-ray diffraction (XRD) and hardness tests were performed.

3.5.1 Cutting Machine

The cutting machine Buehler IsoMet 4000, shown in fig. 4.7, was used to cut the specimens to obtain samples for the fracture surface examination and other littler samples that were used for different tests, such as XRD, density measure and optical microscopy. All the specimens were cut at an advancement speed of 2,5 mm/min with a blade speed of 2900 RPM, the blade used was diamond-coated and the cut was carried on with a lubricant emulsion sprayed on the samples to reduce friction and temperature. The sections obtained were cleaned in ethanol in an ultrasound bath for 1 minute, fracture surfaces were bathed for 5 minutes.



Fig. 4.7 Buehler IsoMet 4000

3.5.2 Polishing Machine

After cutting, the specimens were embedded in resin and then they were manually polished by using the polishing machine Mecatech 234 shown in fig.4.8. To achieve a mirror-like finishing surface abrasive papers and abrasive pastes were used. The used SiC abrasive papers were 800, 1200, 2500 and 4000. This operation exploited water as a lubricant and a

mean to evacuate aluminum residues. For the final steps, a cloth with a diamond pastes of 3 µm and 1 µm were used. In this case, a specific lubricant was adopted.



Fig. 4.8 Mecatech 234

3.5.3 Chemical Etching

Some samples were etched after polishing to better show the microstructure. Chemical etching selectively corrodes metal on the surface to highlight details of the microstructure. The chosen reagent was Keller's reagent, its chemical composition was 2,5 ml HNO₃, 1,5 ml HCl, 1,0 ml HF and 95 ml of water. A droplet of the acidic solution was placed on the surface of half the samples for 20 seconds, then it was washed in ethanol and dried. Only half of the samples was interested in the etching because we observed that the reactant removes some Fe precipitates in the matrix, and therefore changes the sample composition.

3.6 Optical Metallographic Microscope

The optical metallographic microscope is a device used to observe and study the microstructure of metals and metallic alloys. This study includes information on the size

and shape of crystal grains, the porosity, the presence of cracks, inclusions and segregation of precipitates. Samples need to be mirror-finished to be observed and appreciate the minute details such as inclusions and grain boundaries. The main limits of this technology are the relatively limited resolution, (less than 0,2 µm) and the reduction of the field depth with higher magnification, that requires samples to be perfectly planar to be focused.

In this thesis, the Leica DMI 5000 M microscope was used to analyze the porosity and the microstructure of the two different alloys and related manufacturing process. The porosity percentage was calculated with image analysis software "ImageJ" from pictures at 200x magnification. The microscope is shown in fig. 4.9.

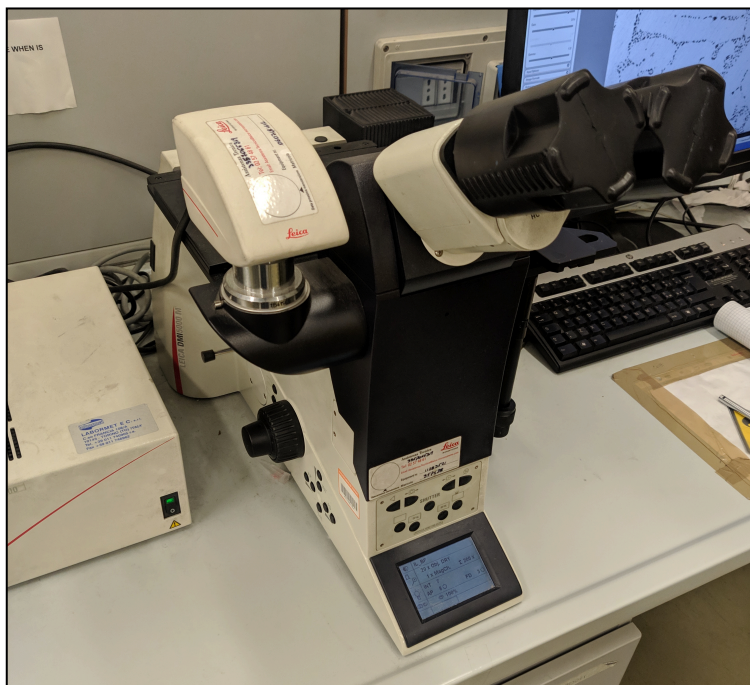


Fig. 4.9 Leica DMI 5000 M

3.7 FESEM (Field Emission Scanning Electron Microscope)

A Scanning Electron Microscope (SEM) is an instrument able to examine the morphology and the microstructure of a sample using an electron beam as a mean of investigation, instead of photons like in an optical microscope. In contrast to the optical microscope, a SEM provides higher magnification and depth field, so it is possible to analyze non planar surfaces such as fracture ones. As SEM works with a collimated electron beam, vacuum

inside the chamber containing the specimens is necessary in order to avoid collisions between the gas molecules and the electrons, which would compromise the image acquisition. In a typical SEM, an electron gun is used to generate the electron beam. When a potential difference is applied to the filament cathode (it can be made of tungsten or lanthanum hexaboride), an electron beam is thermo-ionically emitted. This means that the filament is heated by the Joule effect and, when the electrons receive enough thermal energy to overcome the energetic barrier, they are emitted. In a FESEM, the electron beam is generated by field emission source and accelerated in a high electrical field gradient: an electric field is applied to the emitting metal in a way to deform the bands of the material and allow the emission of electrons by the tunnel effect. The field emission technology produces a smaller and more coherent beam allowing for better magnification and resolution. The electrons emitted are accelerated by an electric field. The beam is then focused on the surface of the specimen with electromagnetic lenses; by modulating the magnetic field it is possible to deflect the beam and scan the entire surface. A scheme of an SEM is shown in fig. 4.10.

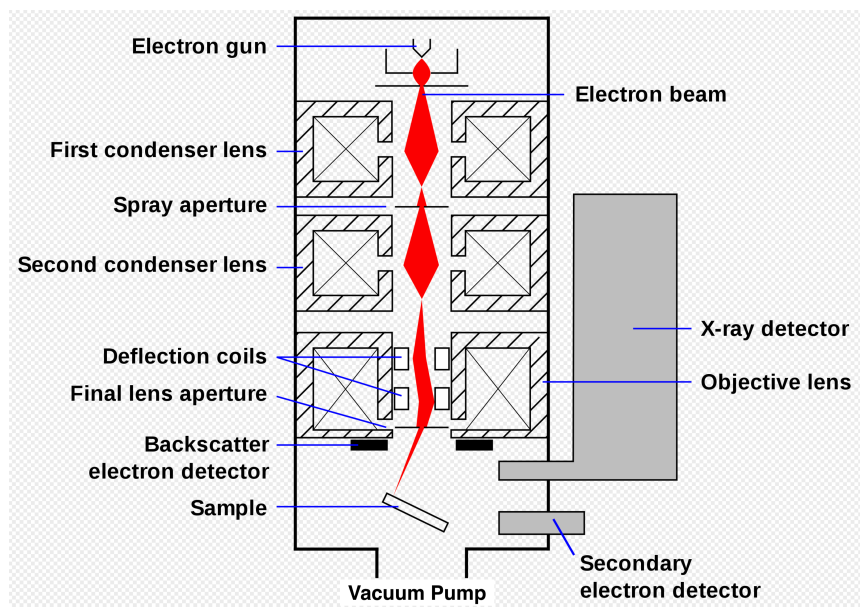


Fig. 4.10 Typical SEM schematics

When the electron beam impacts with the matter there can be elastic and anelastic impacts. The elastic impacts do not modify the kinetic energy of the electrons, on the contrary the anelastic ones transfer energy to the specimens causing a reduction in the kinetic energy of the electron beam. When the beam and the sample interact together they create electron

signals that are detected and elaborated to create an image in grayscale. The typically used signals in electron microscopy, shown in fig. 4.11, are:

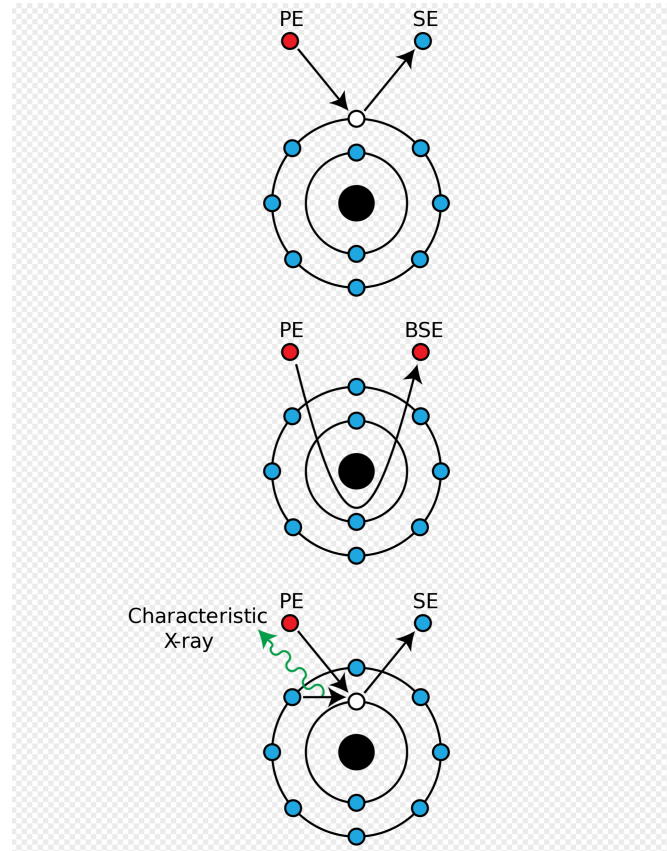


Fig. 4.11 Electrons emission in electron microscopy

Secondary electrons (SE): these electrons are emitted when there is an anelastic interaction between the sample and the beam. They are typically low energy particles ($<50\text{eV}$). They are generated on the surface layer of the sample (10nm depth) so they give mostly information about the morphology.

Backscattered electrons (BSE): BSE comes from elastic interactions and involve a deeper part of the sample. The BSE signal provides more information about the composition of the specimen: the number of BSE depends in fact on the atomic number Z of the encountered atoms. Samples containing component with lower Z phases will result darker in comparison to higher Z phases that will be lighter.

X-rays: when a primary electron interacts with the core level of an atom, an SE is emitted and a gap is created. So a higher energy electron falls in the created gap and emits an X-ray; every chemical element emits its own characteristic wavelength. The EDS (Energy

Dispersive X-ray Spectroscopy) detector is used to analyze the spectrum emitted by the sample and identify the elements contained.

The FESEM used in this thesis work was a ZEISS MERLIN, shown in fig. 4.12, equipped with an EDS Oxford INCA. This was used to observe and investigate the fatigue fracture surfaces and the microstructure of both casted and additive manufactured samples; the EDS was used to investigate the composition of the various phases.



Fig. 4.12 Zeiss Merlin FESEM

3.8 XRD (X-ray Diffraction)

The XRD is a non-destructive technique used to analyze crystalline materials. It allows to identify the main crystalline phases existing in the material and provides information about

their crystal structure. This instrument provides a diffraction pattern that shows the X-ray intensity as a function of the 2θ angle. By comparison with a database, it is possible to identify the various crystal phases contained in the material. The peaks in the graph are caused by constructive interference between the monochromatic X-ray beam and the crystal lattice of the sample.

Constructive interference occurs when the scattered rays are in phase; in this condition Bragg's law (equation 4.1) is satisfied.

$$n\lambda = 2d \sin \theta \quad (4.1)$$

Where λ is the wavelength of the radiation, d is the distance between two adjacent crystal planes and θ is the incident angle. A simple schematic is shown in fig. 4.13[19].

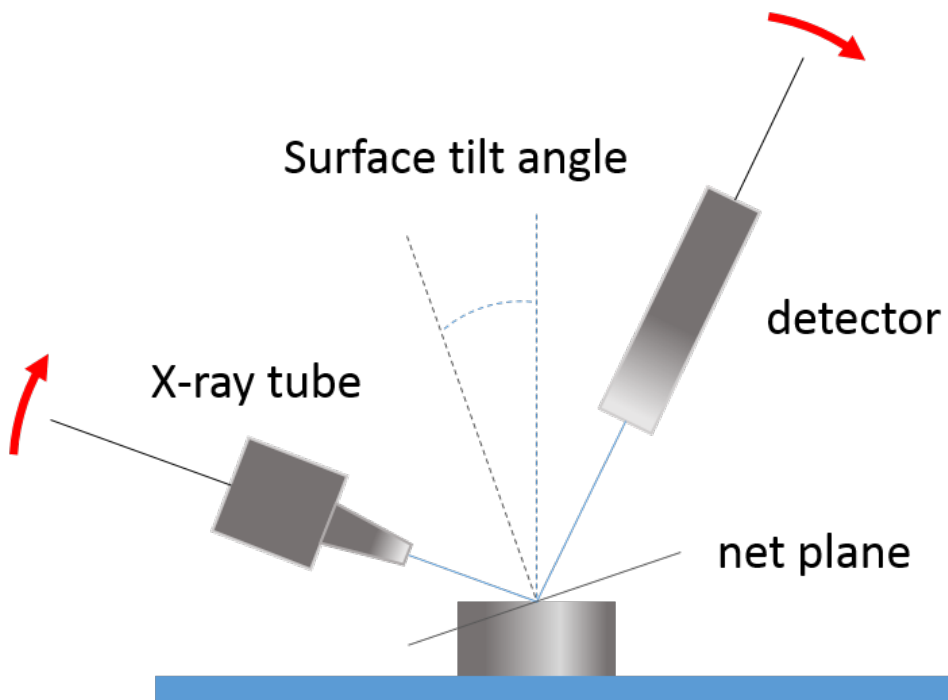


Fig. 4.13 X-ray diffraction scheme

The X-ray beam is created in a cathodic tube. A thermo-ionically electronic beam is accelerated towards a metallic target, it interacts with the electrons of a target emitting X-ray. X-rays are subsequently filtered to obtain a monochromatic beam. The typical metal target is Cu $K\alpha=1,5418 \text{ \AA}$.

The XRD analysis was performed at Politecnico di Torino with a diffractometer Panalytical X'PERT PRO PW3040/60 with Cu $K\alpha$ radiation at 40 kV and 40 mA. The 2θ angle range

varied from 20° to 110° with incremental steps of 0,013°. XRD was performed on both the cast and the AM samples to investigate if any differences in term of crystalline phases exists.

3.9 Hydrostatic Scale

The hydrostatic scale is a scale used to determine the density of a solid and its porosity. The scale is modified with a double plate, one can weigh the sample in the air the other can weigh it in the water. An example is shown in fig. 4.14

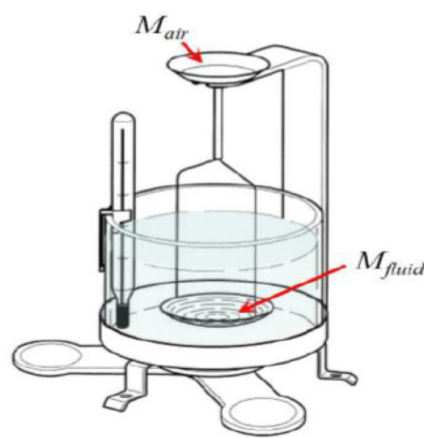


Fig. 4.14 Hydrostatic Scale

The samples must be smoothed with abrasive paper to avoid the influence of surface roughness. When immersed in distilled water the sample fills its open porosity. The sample is weighed firstly in air; secondly it is immersed and then weighed in the water. After that the sample is extracted from the liquid, the drops on the surface are removed with a wet cloth, and it is weighed again with the porosity filled by water. By using these three weights, it is possible to calculate the density of the material according with equation 4.2.

$$\rho = \frac{W_{air} \cdot \rho_{H_2O}}{W_{sat} - W_{H_2O}} \quad (4.2)$$

Where W_{air} is the weight of the sample in air, W_{sat} is the weight of the sample with saturated porosities and W_{H_2O} is the weight in water.

3.10 Brinell Hardness

Hardness measurements are used to determine the resistance of a material to indentation. Usually, the hardness value is related to the tensile strength of a material; the harder is a material, higher is the strength. The hardness test is a non-destructive test that consists of pressing a penetrator on the surface of the metal with a known load to create an imprint. Then, by measuring the imprint size, the instrument produces an empirical value of hardness. The standard that is used as reference to perform a Brinell test is UNI EN ISO 6506-1[20]. This consists of imprinting a sphere of diameter D made of tempered steel with a known load F for a determined lapse of time, and then to measure the diameter d of the imprint on the part. In order to consider the test valid, the applied load F must meet the condition reported in equation 4.3.

$$F = K \cdot D^2 \quad (4.3)$$

where K is a constant of the examined material; for example, the K factor of Al alloys is 10. Furtherly the imprint diameter d must be in the range between 0,24D e 0,6D and the thickness of the piece should be at least 8 times the depth of the imprint. The penetrator must be kept on the surface for 10 to 15 seconds. To meet these specifications the hardness test chosen was the HB 5/250, which means D = 5mm with a load of 250kg applied for 10



Fig. 4.15 Wolpert dia Testor 3b 1973

seconds. The test was performed in the CRF fatigue laboratory in Orbassano with a Wolpert dia Testor 3b shown in fig 4.15.

A sample for every set of measurement was tested to verify the homogeneity of the treatments. The diameter d was calculated as the average of two perpendicular diameters of the imprint; the value of hardness was obtained with a database that related d with the Brinell Hardness.

3.11 Plane Bending Fatigue test

The fatigue test is a destructive test suitable to evaluate the resistance of the material to cyclic stresses. It was carried on using a vibrophore that cyclically stresses the samples. The results obtained were analyzed using the staircase method.

A vibrophore is a resonating machine that can perform high-frequency fatigue test; the used vibrophore was a RUMUL Cracktronic 8204 with a flexion load cell RUMUL spmgs 070.1 of 160Nm. It works with a bending moment so, in order to estimate the value of applied stress is necessary to calculate the Flexural Strength Module (W_f) of the section according to the equation 4.4

$$W_f = \frac{b \cdot h^2}{6} \quad (4.4)$$

Where b is the base and h is height.

In the case of the sample we tested, the section is rectangular. Afterwards, it is possible to calculate the flexural moment required to apply a determined σ to the sample using equation 4.5.

$$M_f = W_f \cdot \sigma \quad (4.5)$$

The specimens were measured with a micrometer before starting the test, in order to verify their dimensions. The size, together with the required stress, were therefore used to calculate W_f . The vibrophore worked at a frequency of 82 Hz; the test is stopped when the sample reaches 10 million cycles or when the frequency dropped to 72 Hz (in this case it means that a crack was propagating catastrophically causing the failure of the sample). Eventually, the samples were manually broken using a hammer to reveal the fracture

surface. The test was performed with $R = 0$ where R is the stress ratio defined as minimum stress/ maximum stress.

A value of R equals to 0 means that the sample is stressed only by traction and the compression stress is zero.

The adopted vibrophore is shown in fig. 4.16.



Fig. 4.16 RUMUL Cracktronic 8204

3.11.1 Staircase method

The staircase method is a statistical approach used to determine the fatigue limit. This method is defined by the standard UNI 3964[21]. The staircase method or Dixon-Mood method provides the mean value of the fatigue limit and an estimate of the deviation of the distribution. At least 15 samples are needed to obtain a reliable value. Some steps of stress amplitude are chosen around the supposed fatigue limit. The steps must be equally spaced by an arbitrary constant d . The constant d must be in the same order of magnitude of the deviation s (between 0,5 s e 2 s), typically used values of d are $d = 10 \text{ N/mm}^2$ or $d = 20 \text{ N/mm}^2$. The samples are then tested at the various steps to the determined number of cycles (in this case 10^7) following this criterion. If the first sample subjected to a stress amplitude near the fatigue limit fails, the following sample will be tested at the step of stress amplitude immediately below. If the sample does not fail (it is called a run-out) the following sample will be tested at the step of stress amplitude immediately above. The test continues until all

the samples are tested. To calculate the mean value of the fatigue limit (it corresponds to a 50% chance of failure) only the results of the least frequent event are used. The mean value can be calculated with equation 4.6

$$\sigma_D = \sigma_0 + d \left(\frac{A}{N} \pm 0,5 \right) \quad (4.6)$$

where σ_0 is the lowest step in the staircase, d is the spacing between the steps, $N = \sum n_i$ is the total number of the least frequent events, $A = \sum i \cdot n_i$ is the sum of the products of the number of events (least frequent events) that are present for each step multiplied by the order number of the step. The number of the step is counted from the lowest one that has the number 0. Between the parenthesis, if the least frequent event is failure, it is used the minus sign. If the least frequent event is run-out, the plus sign is used instead. The estimation of the deviation is calculated with equation 4.7

$$s = 1,62 d \left(\frac{NB - A^2}{N^2} + 0,029 \right) \quad (4.7)$$

where $B = \sum i^2 \cdot n_i$

A typical test sheet is shown in fig. 4.17.

Level	Stress Sa [MPa]	SEQUENCE NUMBER OF SPECIMENS																				Numbers of tests		
		1	2	3	4	5	6	7	8	9	10	11	12	13	14	15	16	17	18	19	20			
i																						x	o	
																						0	0	
																						0	0	
																						0	0	
3	118		x																			1	0	
2	109	o		x																		2	1	
1	100			x		x		x		o		x		x								5	1	
0	91				o		o		o			o		o		o						0	5	
																						0	0	
																						0	0	
Nº of cycles $\times 10^6$		10,000	2,070	9,600	1,530	27,000	4,186	10,000	4,581	10,000	14,000	2,492	3,645	10,000	5,314	10,000							$\Sigma r_i =$	$\Sigma l_i =$
																						8	7	
																						r _i	l _i	

Fig. 4.17 Typical staircase data sheet

3.12 Profilometer

To investigate the surface finishing of the specimens used in this thesis, the surface roughness was measured by the CRF technicians using the profilometer Taylor Hobson mod. TALYSURF PLUS, shown in fig. 4.18.



Fig. 4.18 TALYSURF PLUS profilometer

A profilometer measures the height and depth of the peaks and the valleys on the surface of the material. The following parameters were determined by the test:

- Ra: This parameter is the arithmetic average of the distance between peaks and valleys from the mean line.
- Rz: This parameter is the maximum distance between the highest peak and the lowest valley, given a determined length of material L

- R_t : This parameter is the distance between two lines. The first one is obtained from the average of the 5 highest peaks in a determined length L , the second line is the average of the 5 lowest valleys in a determined length L .

The profilometer scans the sample surface using a gauge head in contact with the material that is dragged along a line. The head records the vertical movement providing a measurement of the height of each peak or the depth of each valley. Smaller heads can measure more easily narrow valleys; the smallest heads used can reach dimensions of few tens of nanometers.

3.13 Tensile test

The tensile test is a destructive test that allows to determine various mechanical properties of the material. In fact, it is possible to obtain the values of tensile strength (R_m), yield strength ($R_{p0,2}$), elongation at break ($A\%$) and elastic modulus (E).

The test is performed by applying an uni-axial vertical load on a standard specimen. The standard that defines methods and materials to be used for this kind of test is the UNI EN ISO 6892-1 for metals[22]. The test can be performed in strain control or stress control. In the first case, strain control, the deformation rate is constant, and the load increase is measured. On the contrary, the second case uses a constant load rate increase and measures the deformation. The most common is the strain control test. By following the ISO standard, the samples can show rectangular, square or round section. Their size must satisfy the conditions reported in equation 4.8 between length and section area.

$$L_0 = k \sqrt{S_0} \quad (4.8)$$

Where k is a proportionality coefficient with a value of 5,65. L_0 is the length of the part of the specimen with reduced section and S_0 is the section of this part of the sample as shown in fig. 4.19.

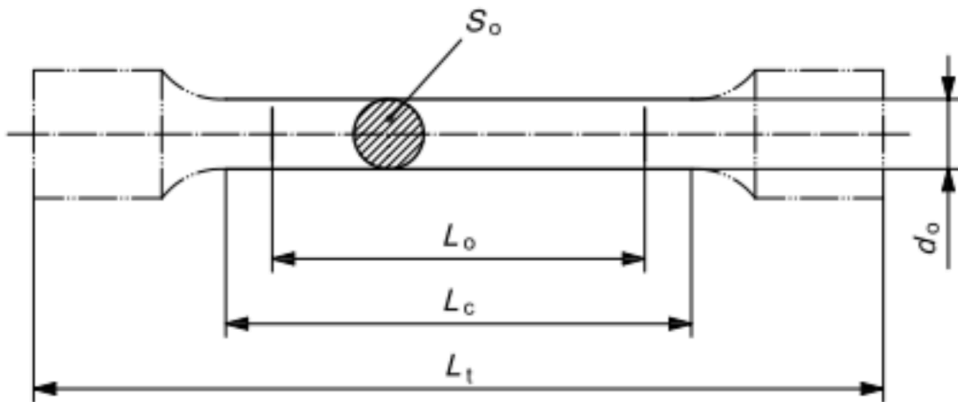


Fig. 4.19 Geometry of a tensile sample

The tensile tests were performed in the CRF laboratories using a Zwick 1474 machine with a Zwick load cell 100 kN, shown in fig 4.20. The tested specimens had round section and threaded heads; this allows them to be screwed and therefore anchored to the machine. The test was performed at room temperature in strain control conditions, with a stress rate of $0,00025 \text{ s}^{-1}$.



Fig. 4.20 Zwick/Roell 1474

The tensile test provides a graph that relates the stress σ and the strain ε .

The stress is calculated according the equation 4.9

$$\sigma = \frac{F}{A_0} \quad (4.9)$$

where F is the load applied in N and A_0 the nominal section of the sample.

The strain is calculated with equation 4.10

$$\epsilon = \frac{\Delta L}{L_0} \quad (4.10)$$

where ΔL is the difference between the final length L and the nominal initial length L_0 .

4. Experimental results

The following chapter presents the experimental results obtained in this work of thesis. The work started with the analysis of chemical composition and microstructure to investigate the differences between the two alloys resulting from different processing paths. Subsequently, the physical properties were studied in order to define the main characteristics of the specimens. These tests were followed by mechanical tests to study how all these characteristics influence the behavior of the samples. Finally, the morphology of the fracture surfaces was observed to gain further information on the failure and the mechanics of it.

4.1 Microstructure and chemical composition of Al-Si-Mg alloys

The two hypoeutectic alloys studied in this work have similar composition, but they differ for the amount of silicon. The two compositions are shown in tab 5.1. They have been investigated by XRD and EDS techniques to check the differences between them.

Elements %	Si	Mg	Fe	Ti	Cu	Ni
AlSi7Mg	6,5/7,5	0,2/0,65	max 0,55	max 0,25	max 0,2	max 0,15
AlSi10Mg	9/11	0,2/0,45	max 0,55	max 0,15	max 0,05	max 0,05

Tab 5.1 Compositions of AlSi10Mg and AlSi7Mg

4.1.1 XRD

This paragraph compares the XRD spectra of the cast sample and the SLM sample to investigate possible differences. The XRD analysis shows peaks due to the crystalline phases present in the sample. In fig. 5.1 is possible to see the two spectra, they both show the same peaks of Al (ICDD card n. 00-004-0787) and Si (ICDD card n. 01-080-0018) meaning that the same phases are present in both samples and there are no substantial differences in the crystalline structure. The Mg contained in both alloys does not show up in the XRD patterns because its percentage is below the sensitivity of the XRD technique, for the same reason the hardening phase Mg₂Si is not visible either.

Both samples were heat treated according to a T6 treatment (solution, quench and artificial ageing). It was expected that the same heat treatment should lead to similar results in terms of microstructure and mechanical characteristics, even though the samples were manufactured with different methods.

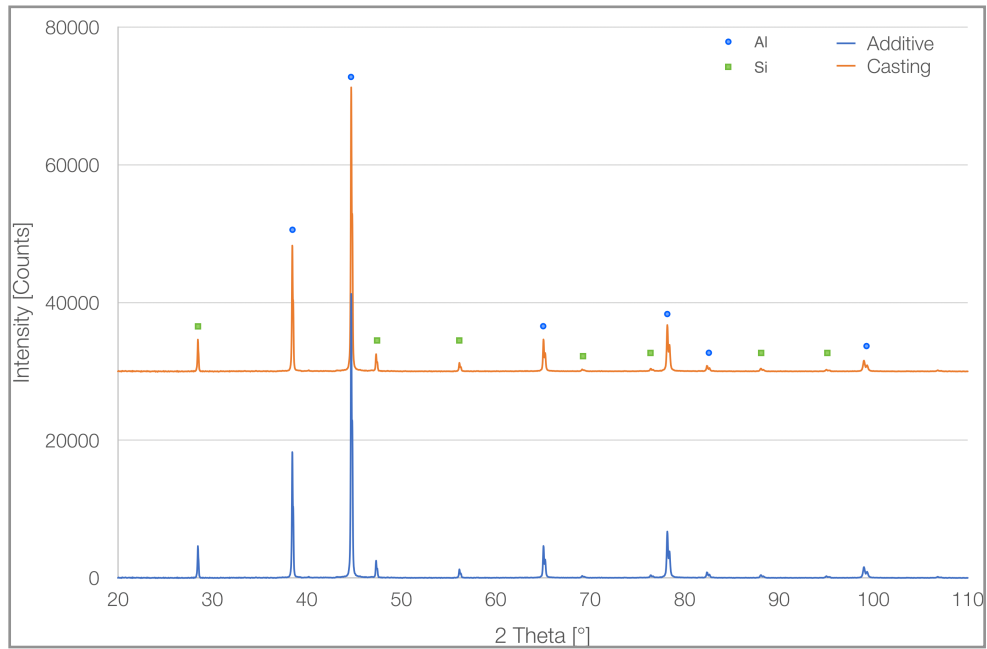


Fig. 5.1 XRD spectra of additive and casting samples

4.1.2 Microstructure

The microstructure was observed with the metallographic microscope and the FESEM. The two alloys, before heat treating, presents radically different microstructures. Casting produces dendritic structures and segregation of Si at grain boundaries. AM produces the typical melt pools and a much finer structure. The differences between the two are shown in fig. 5.2.

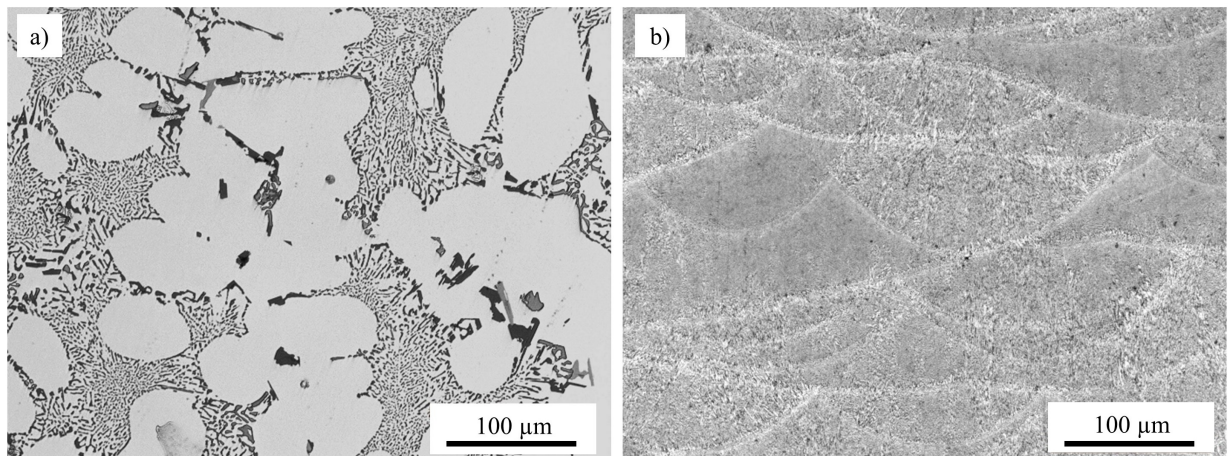


Fig. 5.2 Micrography taken by optical microscope, (a) cast sample with dendritic structure and Si segregation, (b) AM sample with melt pools[23]

Both samples were heat treated with a T6 treatment and this can explain why the structure and somehow similar, with an Al matrix and Si segregation.

The main differences are due to the processing method. As it is possible to observe in fig 5.3 the cast sample (a) presents a structure characterized by the segregation of larger Si grains at the grain boundaries of the large Al crystals, that is in the zones where a dendritic structure formed just after the casting. While the AM sample (b) shows a finer and more homogenous distribution of Si crystals.

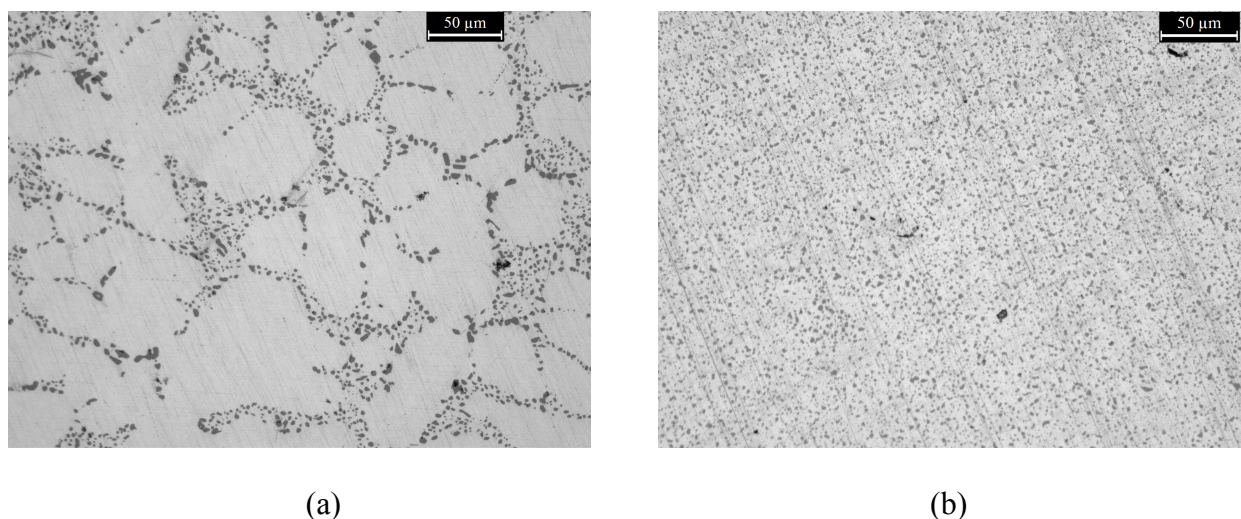


Fig. 5.3 Micrography taken by optical microscope, (a) cast sample and silicon grains formed inside the former dendritic structure, (b) AM sample with homogeneous distribution of silicon crystals and some porosity

The porosity was evaluated with image analysis software "ImageJ". Samples processed by SLM and casting showed similar results with an average porosity of 0,49% for AM and 0,45% for casting. The main difference is the porosity distribution inside the microstructure shown by comparing the porosity percent measured in different zones and calculating the standard deviation. In fact, the AM sample showed the very little standard deviation of porosity percent of 0.015, meaning that the porosity is small and homogeneous, whereas the cast sample showed a wider distribution of porosity percentages with a standard deviation of 2.209 , meaning that the pores are rarer but bigger in size. It is shown in fig. 5.4. The larger pore-size in the casting sample is expected to decrease the fatigue resistance because big pores can act as crack initiator. Also the inclusions shown in fig 5.4a are not present in the AM alloy, inclusions of this size can have a detrimental effect on fatigue resistance.

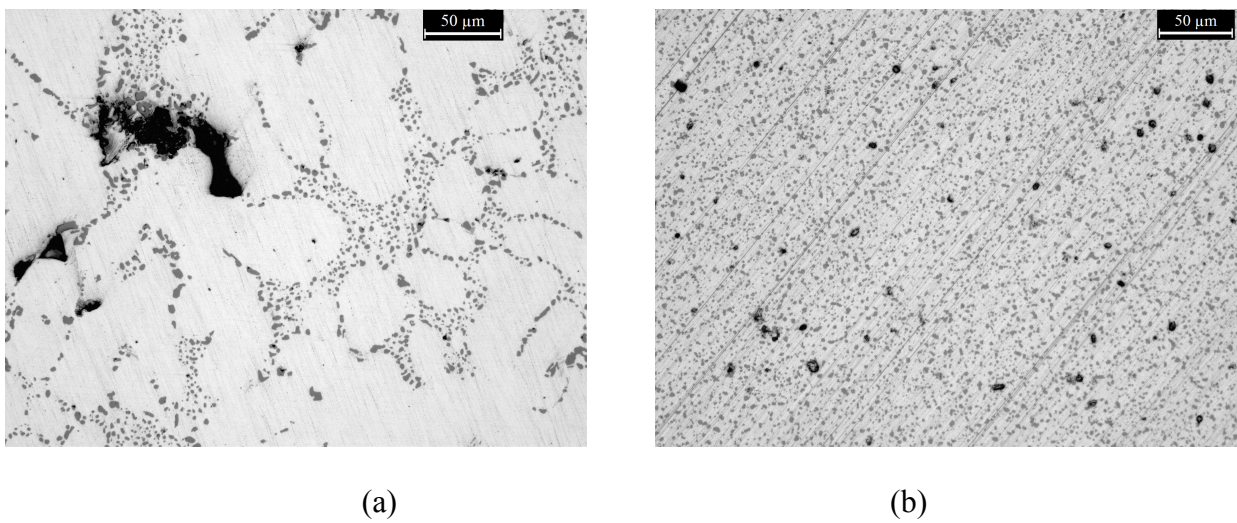
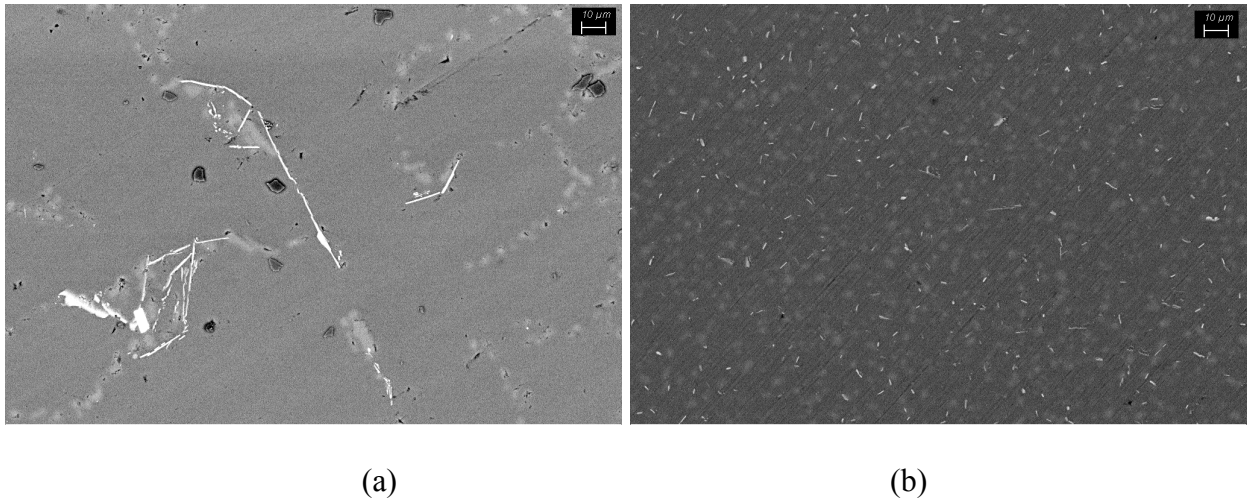


Fig. 5.4 Micrography taken by optical microscope, (a) cast sample with big porosity and inclusion, (b) AM sample with homogenous porosity distribution

Investigating the microstructure with the FESEM-EDS it was possible to analyze the acicular precipitates in the alloy, which are typical of the Al-Si casting alloys. Both samples (AM and cast) present this Fe-based precipitates but the morphology changes depending on the processing path. It is possible to observe in fig. 5.5 how these precipitates are larger and more acuminate in the cast sample (a) while the AM sample (b) presents finer and more homogeneously distributed particles of this type. These precipitates can strongly affect the fatigue resistance, since in Al alloys it is controlled by the size and dimension of hard precipitates. In AM samples their presence can be beneficial and can harden the alloy because they are well distributed, while in cast samples they can act as defects and crack initiators.



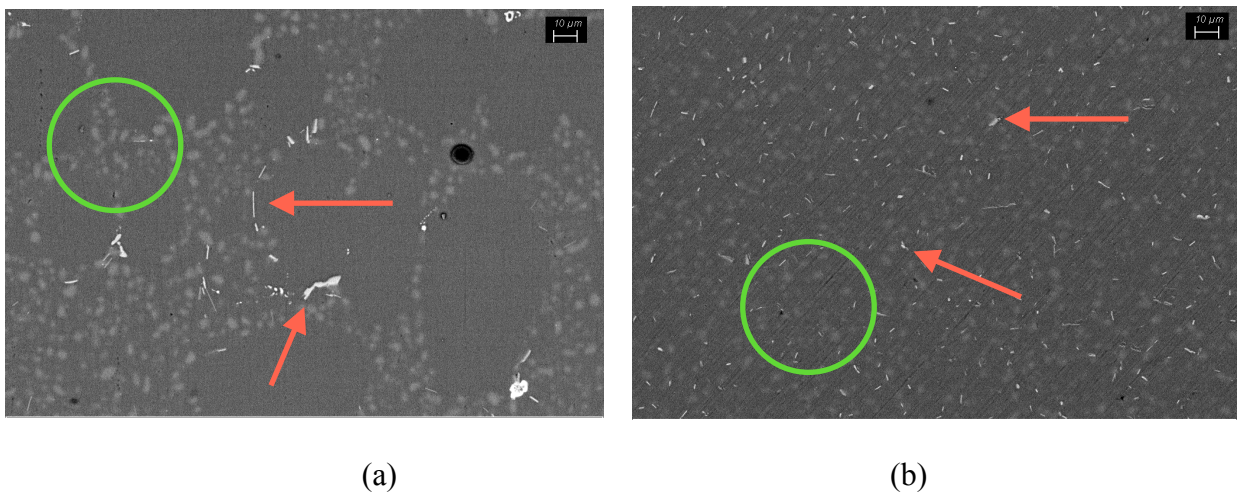
(a)

(b)

Fig. 5.5 FESEM images of the microstructure showing acicular precipitates containing iron: (a) cast alloy, (b) SLM sample

4.1.2 EDS

The EDS analysis was performed on mirror polished samples observed in the FESEM. This showed a similar microstructure, however the casting sample showed a coarser one with bigger precipitates and more silicon segregation, even though the Si percent is lower, as shown in fig. 5.6



(a)

(b)

Fig. 5.6 FESEM images of the microstructure: (a) Micrography of cast sample, (b) Micrography of AM sample

It is possible to observe in fig. 5.6b how the white precipitates, highlighted by the red arrows, are bigger than the same in the AM micrography (5.6a). The light spots due to silicon grains, highlighted with the green circles, are more homogenously distributed in the AM sample, whereas in the casting it is still possible to observe their segregation due to the manufacturing process. In fact, this segregation is observable also when analyzing the chemical composition of different parts of the microstructure by SEM-EDS. The results are presented in tab 5.1.

Element	Spect. 1	Spect. 2	Spect. 3	Spect. 4	Spect. 6	Spect. 7	Spect. 8
	A%						
O		4,59		11,60			
Mg	0,18	0,30		0,42	0,29		0,42
Al	64,27	79,36	25,46	77,46	83,66	4,74	98,45
Si	26,75	9,30	75,54	10,53	9,16	95,26	1,13
Fe	8,80	6,46			6,88		

Tab 5.1 Atomic % of elements in different parts of the samples

The EDS results shown in tab 5.1 are related to fig. 5.7, that shows in which area of the sample the EDS analysis was performed.



Fig. 5.7 EDS analysis on the samples, (a) AM sample, Fe-rich precipitates, Al matrix and Si grains at the Al grain boundaries, (b) Cast sample, Fe-rich precipitates, Al matrix and Si grains segregation at the grain boundaries of rather large Al crystals.

From the data in tab 5.1 is possible to observe that in spectra n°2 and n°4 some oxygen is present, those are both in the AM sample and this can be due to the fact that samples were prepared 24h before they were put in the vacuum chamber, so an oxidized layer formed on the surface, whereas the cast sample was prepared just before the microscopic examination and it does not show O in its spectra.

The segregation of Si comes out when comparing spectra 4 and 7 with spectra 4 and 8, which refers to Al and Si crystals respectively. In the zones where Si precipitation occurs the Si to Al ratio was about 75% to 24% for AM sample (spectrum 3) and 95% to 5% for cast samples (spectrum 7). The acicular precipitates observed were composed by Fe, Mg, Al and Si, but they showed different composition and dimensions in case of AM and cast samples (spectra 1,2 and 6). In the AM sample these precipitates were richer in Fe and Si and finer (they are less than 10 μm in size, as shown by the scale bar), whereas in the cast sample the precipitates were bigger than the 10 μm scale bar. The presence of acicular hard precipitates and their size can influence the fatigue behavior of the alloy.

4.2 Physical Properties

Other physical properties of the samples were investigated to put in evidence possible differences between them. This study involved density and surface roughness. The porosity level, already been discussed in the microstructure paragraph, should be compared with the density measurements. Differences in these values could help to understand the material fatigue behavior.

4.2.1 Density

The density of both samples was measured with a hydrostatic balance and compared with the theoretical one. The theoretical density used in the calculations was 2,69 g/cm³. The Si percentage modifies the density of the aluminum alloy, but the difference in the composition of these two alloys is not big enough to significantly change the density value. The results are presented in tab. 5.2.

Sample	Theor. ρ	Measured ρ	Relative ρ	Std dev
	g/cm ³	g/cm ³	%	
Cast h04	2,69	2,6775	99,538	0,007
Cast h15	2,69	2,6802	99,606	0,004
AM a04	2,69	2,6371	98,052	0,002
AM a 05	2,69	2,6409	98,166	0,003

Tab. 5.2 Relative densities

Each value of measured ρ was the average of 3 tests. The density of the cast samples is higher, this can be due to less total porosity, even if the pores are bigger (already mentioned in the previous paragraphs) whereas the AM material shows more cavities inside. The standard deviation values are very small meaning there is no dispersion in the data obtained. Probably improving the building parameters of the SLM technique or adding a post-processing step such as HIP, it should be possible to achieve better density results for the AM products. This could furtherly improve the mechanical properties of the alloy.

4.2.2 Surface roughness

Surface roughness has the highest influence on fatigue behavior, especially on bending fatigue tests. Indeed, the plane bending test was chosen to exalt the surface contribution to fatigue resistance. The three samples were tested by CRF and showed very different values of surface roughness, the results are presented in tab 5.3. All the results are an average of different measurements to give a picture of the whole component.

Sample	Ra	Rt	Rt
	μm	μm	μm
Cast	0,253	2,45	1,98
AM as built	16,193	125,95	87,85
AM Tumbled	5,286	46,688	39,449

Tab. 5.3 Surface roughness values

The casting samples were obtained by machining a cast object, so that the surface finishing was very good, while the AM samples show a more rough surface that should lower sensibly the fatigue resistance. This hypothesis was not confirmed by the fatigue test. As shown in fig 5.8(a) the surface of the AM parts is rough because constituted by a layer of semi-sintered powders, that could not act as notches on the surface to initiate a crack but rather as simply attached particles on the surface. In addition, it is shown in 5.8(b) the same surface after the tumbling treatment, that removed the not well sintered particles and thus allowed to obtain a smoother finishing.

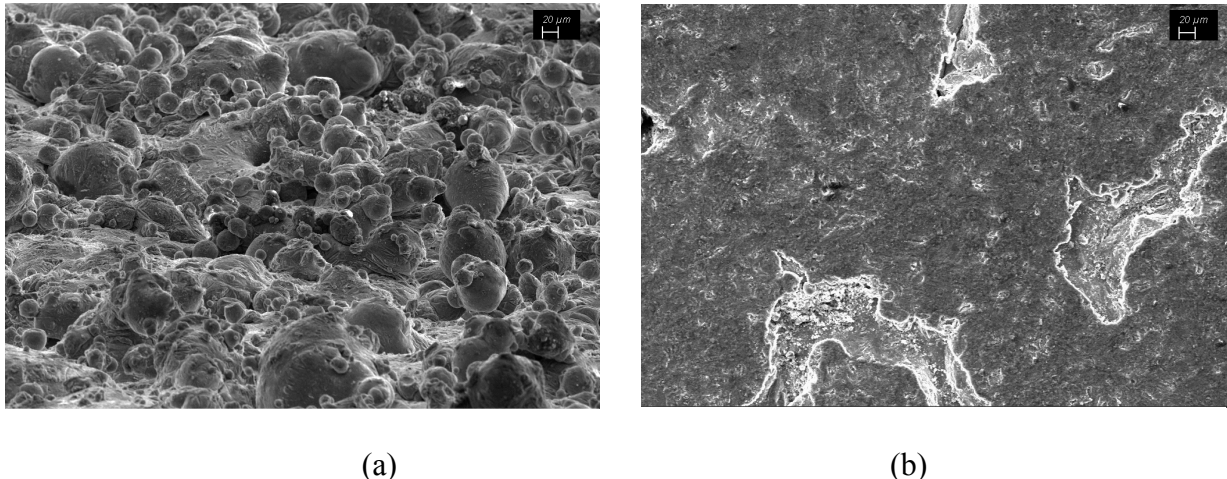


Fig. 5.8 FESEM images of the surface of SLM samples, (a) as built, (b) tumbled

The tumbling was conducted for 35 minutes at 250 RPM with ceramic bodies and 15% of water as a lubricant causing the surface wear. It must be noted that even with the tumbling finishing the surface roughness of the AM samples still remained higher than that of cast and machined samples. This surface finishing could be furtherly improved to achieve even better results in fatigue resistance.

4.3 Mechanical properties

The mechanical properties were measured to have a mean of comparison between this thesis work and the previous ones. The tensile strength was measured in heat-treated samples made from both alloys to verify that the mechanical properties were similar. The hardness test was conducted to verify the homogeneity of heat treatments since they were performed on batches of 5 samples at a time.

4.3.1 Brinell hardness

The hardness measurements were performed on one sample taken from each batch submitted to heat treatment. Several indentations were made to average the value obtained. Also some casting sample were tested to compare the two alloys. The results of hardness are presented in tab 5.4.

Provino	HB 5/250
2.05.19	106,9
6.05.19	106,9
7.05.19	106,9
8.05.19	106,9
9.05.19	106,9
13.05.19	106,9
14.05.19	106,9
15.05.19	106,9
Cast	100

Tab. 5.4 HB hardness

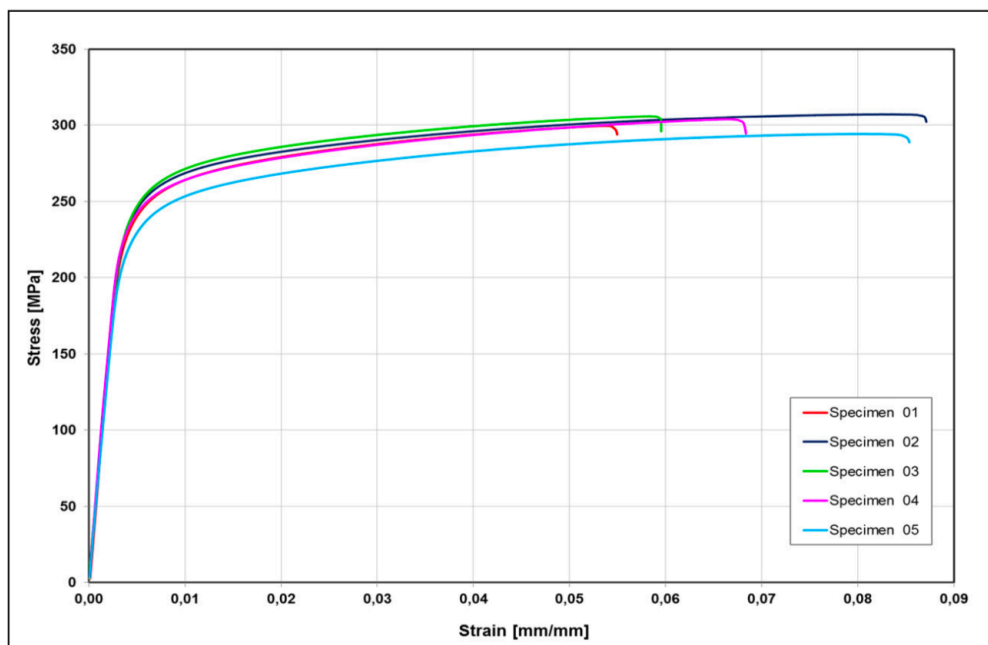
The result obtained for cast Al-Si samples is an average of 5 measurements, however, all gave the same results so that there is no dispersion in the data. The results obtained for AM samples are comparable to the other thesis work [18] on the same alloy and the same treatment, they also show great homogeneity for different groups of heat treated samples. Eventually, the values of cast and AM do not differ significantly meaning that the heat treatment performed on each alloy gave comparable results.

4.3.2 Tensile strength

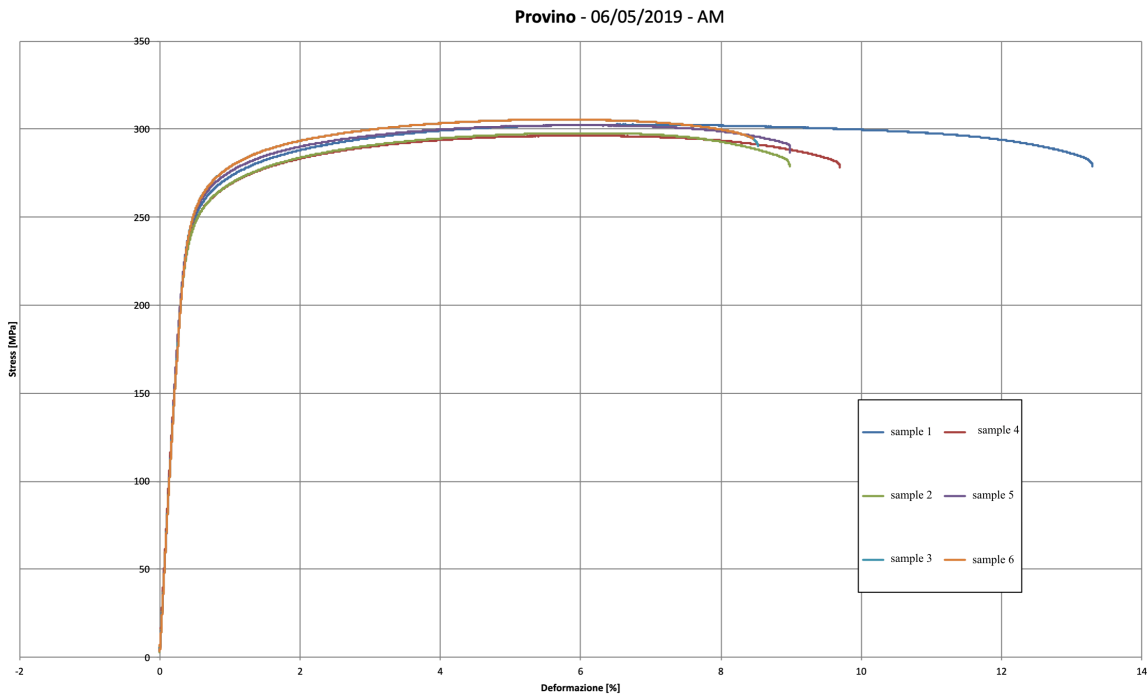
The tensile test was performed to highlight some different behaviors for the two alloys. The results obtained are shown in tab 5.5 while the curves are visible in fig. 5.9.

Provino	d₀	S₀	E	R_{p0,2}	R_m	A
	mm	mm ²	GPa	MPa	MPa	%
1 AM	7,85	48,40	74,1	253,2	302,7	12,9
2 AM	7,85	48,40	75,1	248,9	296,3	9,3
3 AM	7,85	48,40	73,8	249,5	297,8	8,6
4 AM	7,85	48,40	73,5	256,5	302,2	8,6
5 AM	7,85	48,40	75,5	257,3	305,5	8,1
6 AM	7,85	48,40	77,4	257,3	303,8	8,1
Average	7,85	48,40	74,9 ± 1,1	253,8 ± 3,3	301,4 ± 2,9	9,2 ± 1,2
1 Cast	8	50,26	71,781	243,8	299,7	5,11
2 Cast	8	50,26	72,160	249,0	307,3	8,29
3 Cast	8	50,26	74,493	250,0	305,9	5,56
4 Cast	8	50,26	78,407	243,0	304,0	6,46
5 Cast	8	50,26	70,083	232,2	294,3	8,12
Average	8	50,26	73,4 ± 2,5	243,6 ± 4,8	302,2 ± 4,2	6,7 ± 1,2

Tab. 5.5 Tensile test results



(a)



(b)

Fig. 5.9 Stress/strain curves of (a) cast samples and (b) AM samples

There are no major differences in the tensile behavior of the two alloys meaning that they are comparable in terms of mechanical properties. The only difference that is possible to notice is a slight improvement in percentage elongation at break in AM samples showing that this processing method produces minor improvements in ductility. Improved ductility can be a result from a finer microstructure, and it could also increase fatigue resistance.

4.4 Fatigue behavior

The results of the fatigue testing contained in this paragraph are normalized due to corporate confidentiality. The value of cast fatigue limit was considered as 100 and the others are calculated from that. The limit of fatigue was determined in 10^7 cycles. The specimens examined were the cast and machined, the AM as built and AM tumbled. All the specimens were submitted to T6 treatment before the fatigue test. These samples were chosen to investigate the roles of path processing and surface finishing in fatigue behavior. The results obtained are presented in fig 5.10, 5.11 and 5.12.

Job N°:	18R2709
Material:	AISI7Mg0,3-T6
Specimen geometry:	Hourglass
Fatigue test:	HCF - Bending fatigue
Stress ratio:	kt=1,17
Temperature:	R = 0
	Room temperature

**FATIGUE LIMIT
STAIR-CASE METHOD**

Level	Stress Sa [MPa]	SEQUENCE NUMBER OF SPECIMENS																				Numbers of tests			
		1	2	3	4	5	6	7	8	9	10	11	12	13	14	15	16	17	18	19	20	x	o		
i																						0	0	0	
																						0	0	0	
																						0	0	0	
3	118	X																				1	0	0	
2	109	O	X																			2	1	0	
1	100		X	X																		5	1	0	
0	91		O	O	O																0	5	0	0	
																					0	0	0	0	
Nº of cycles x 10 ⁶		10,000	2,070	9,800	1,530	27,000	4,186	10,000	4,581	10,000	14,000	2,492	3,645	10,000	5,314	10,000						Σri =	Σli =		
																						8	7		
																						ri	li		

Ni	i	ixNi	i ²	i ² xiNi
0	0	0	0	0
0	0	0	0	0
0	0	0	0	0
0	3	0	9	0
1	2	2	4	4
1	1	1	1	1
5	0	0	0	0
0	0	0	0	0
0	0	0	0	0
N=	7	A=	3	B=
Ni=ri per Σri < Σli (caso1)				
Ni=li per Σri >= Σli (caso2)				

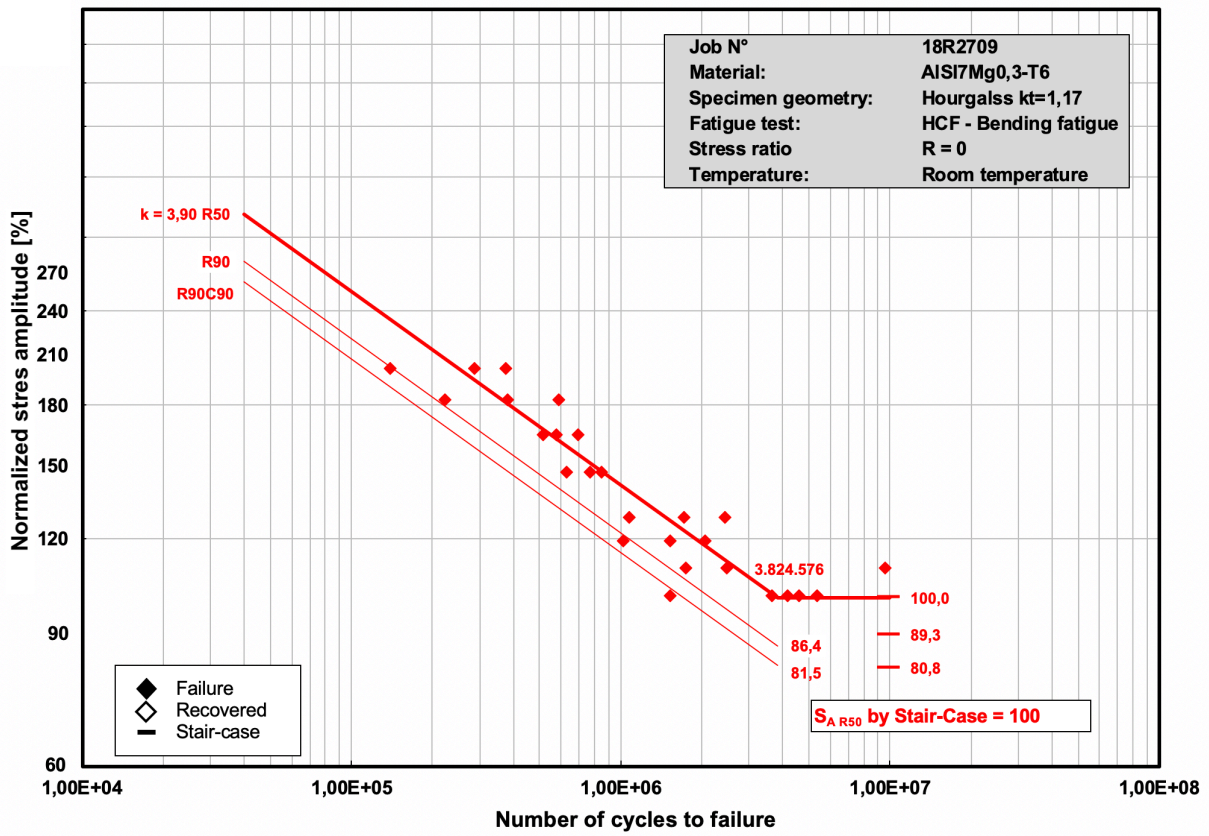
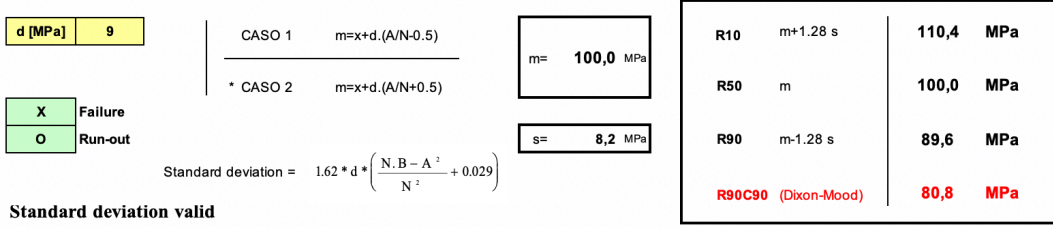


Fig. 5.10 Normalized Stair-case and Wohler's curve for cast samples

Job No:	19R0919
Material:	AlSi10Mg-T6 - As built
Specimen geometry:	Hourgals Kt = 1,17
Fatigue test:	HCF - Flat bending fatigue
Stress ratio:	R = 0
Temperature:	Room temperature

FATIGUE LIMIT STAIR-CASE METHOD

Ni	i	$i \times Ni$	i^2	$i^2 \times Ni$	
0	0	0	0	0	
0	0	0	0	0	
0	0	0	0	0	
1	2	2	4	4	
6	1	6	1	6	
0	0	0	0	0	
0	0	0	0	0	
0	0	0	0	0	
0	0	0	0	0	
N=	7	A=	8	B=	10

$N_i = r_i$ per $\sum r_i < \sum l_i$ (caso 1)

$N_i = l_i \text{ per } \sum r_i > \sum l_i$ (caso 2)

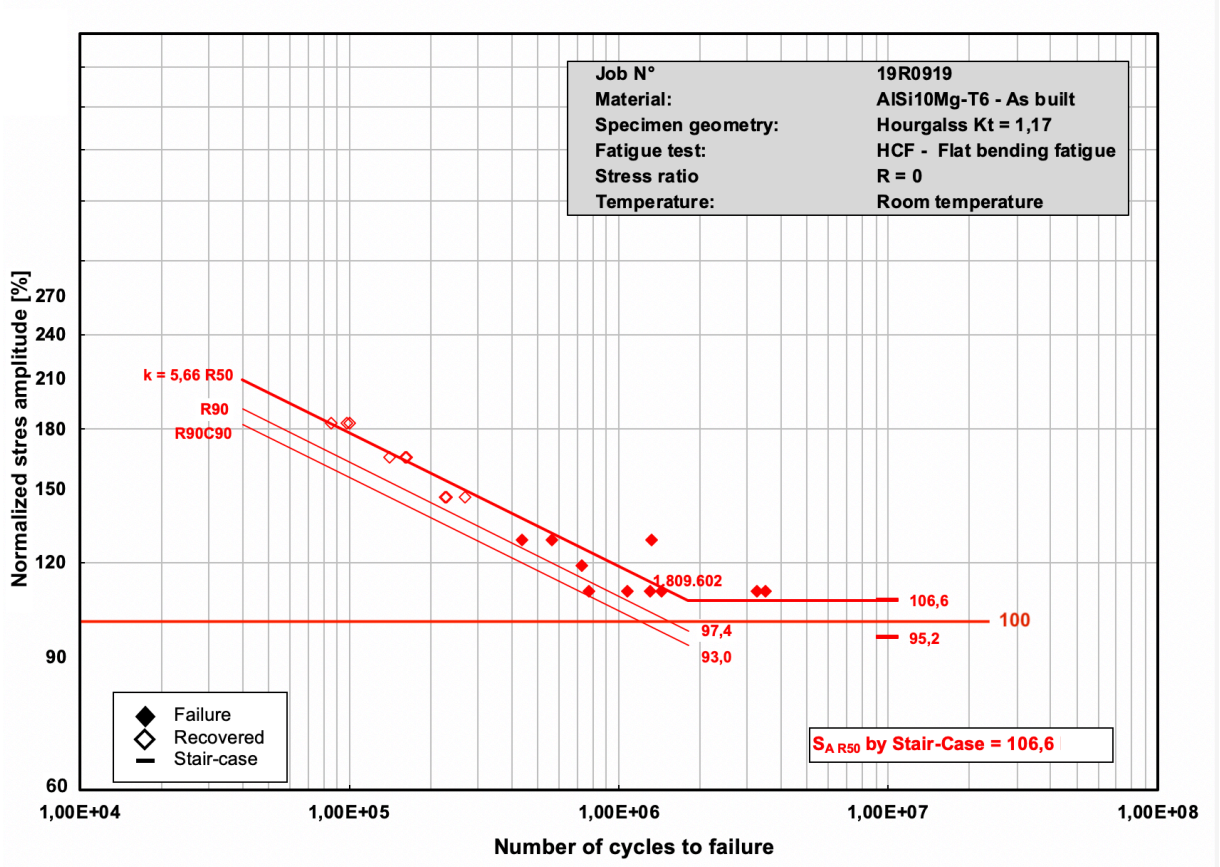


Fig. 5.11 Stair-case and Wohler's curve for AM as built samples, the results are normalized using the casting fatigue limit as 100

Job N°:	19R0919
Material:	AISI10Mg-T6 - Tumbled
Specimen geometry:	Hourgass Kt = 1,17
Fatigue test:	HCF - Bending fatigue
Stress ratio:	R = 0
Temperature:	Room temperature

FATIGUE LIMIT STAIR-CASE METHOD

Level	Stress Sa [MPa]	SEQUENCE NUMBER OF SPECIMENS																				Numbers of tests		Ni	i	ixNi	i^2	i^2xNi
		1	2	3	4	5	6	7	8	9	10	11	12	13	14	15	16	17	18	19	20	x	o					
i																						0	0	0	0	0	0	
																						0	0	0	0	0	0	
																						0	0	0	0	0	0	
1	146,5	X	X	X	X	X	X	X	X	X	X	X	X	X	X	X	X	X	X	X	X	8	0	0	0	0	0	
0	137,4	O	O	O	O	O	O	O	O	O	O	O	O	O	O	O	O	O	O	O	O	0	7	0	0	0	0	0
																						0	0	0	0	0	0	
																						0	0	0	0	0	0	
																						0	0	0	0	0	0	
Nº of cycles x 10 ⁶		0,467	10,000	0,360	10,000	1,239	10,000	0,446	10,000	1,515	10,000	0,294	10,000	0,501	10,000	0,587							Σri =	Σli =	N=	A=	B=	0
																						8	7	n	li			

Ni=ri per Σri < Σli (caso1)
Ni=li per Σri >_ Σli (caso2)

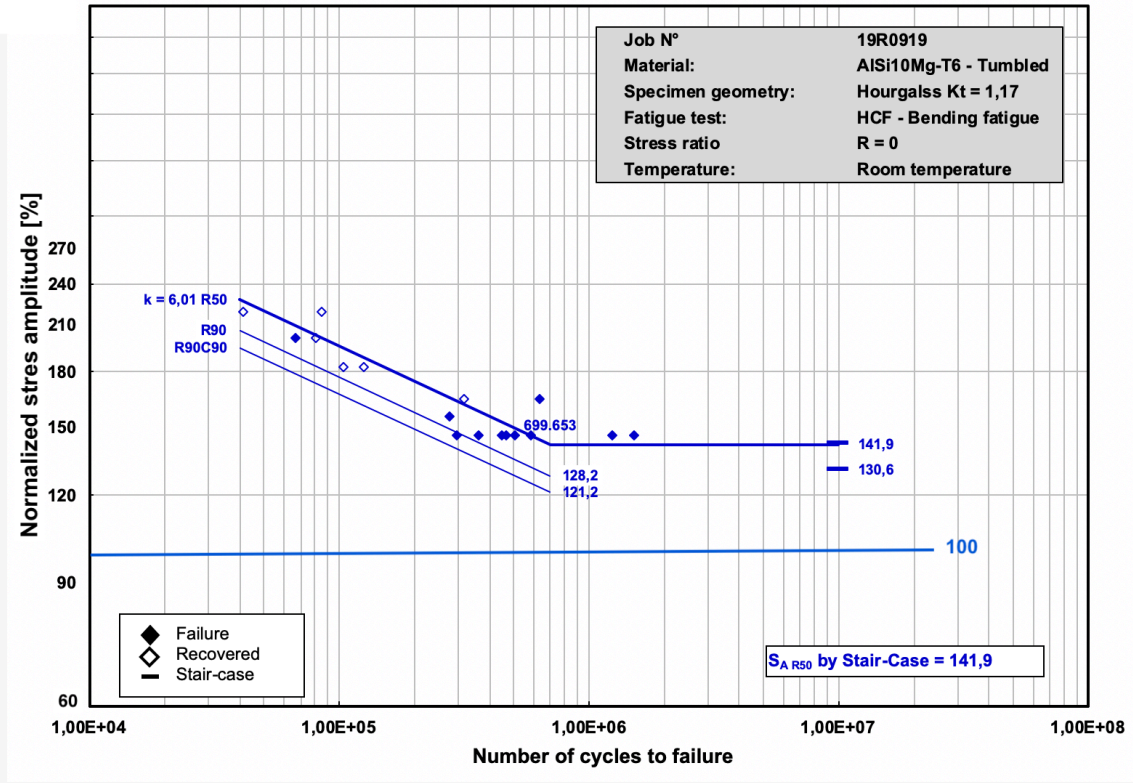
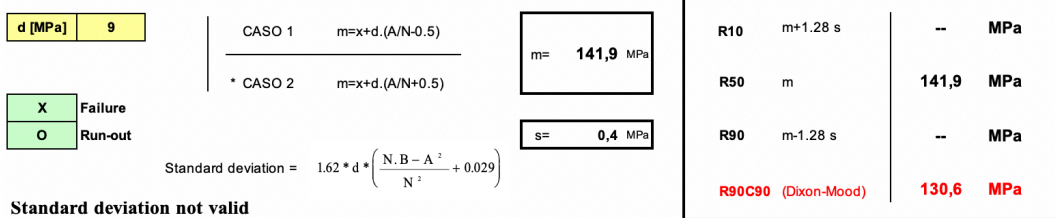


Fig. 5.12 Stair-case and Wohler's curve for AM tumbled samples, the results are normalized using the casting fatigue limit as 100

The results show that even if the cast sample had the best surface finishing its fatigue limit is the lowest. In fact, there is an increase of 6,6% in fatigue limit for the as-built samples and a 41,9% increase for the tumbled samples. The AM process seems to produce better fatigue behavior for the elements previously discussed such as finer microstructure, smaller precipitates and porosity and lack of inclusions. As expected the tumbling treatment on the AM samples produces a good increase in fatigue resistance. For the AM samples, the standard deviation was not valid because the staircase needs at least 4 steps to calculate it, but only three steps were used for testing, owing to the high reproducibility of experimental results. The values found, were indicated with the symbol R_x , where $x\%$ represents reliability. For example, R_{50} means reliability at 50%, i.e. the 50% of samples will survive. The final value indicated as $R_{90}C_{90}$ means reliability at 90% and confidence at 90%. Confidence is calculated on the number of samples used, it is a measure of confidence of the value obtained.

The three Wohler's curve are compared in fig. 5.13 to highlight the differences between the samples.

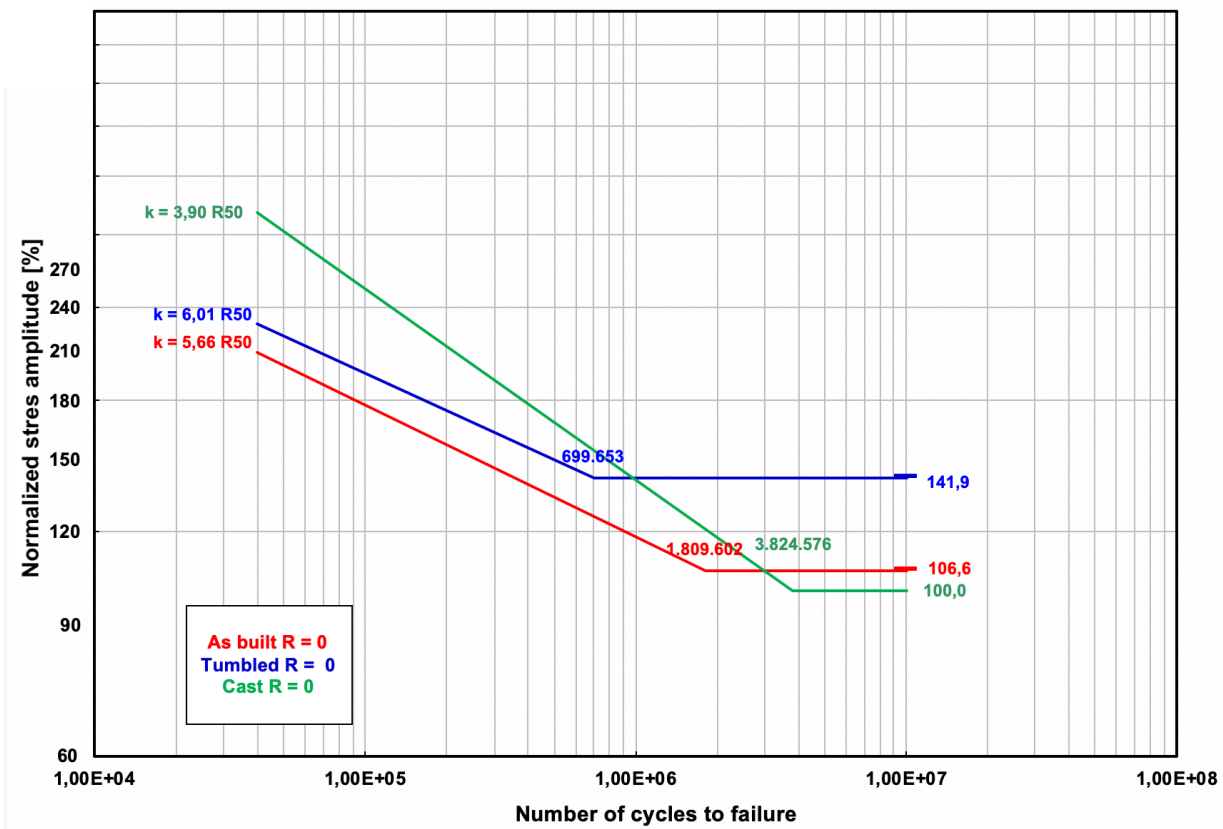


Fig. 5.13 Comparison between Wohler's curve for cast and AM samples

4.5 Fracture surface

After the fatigue testing, the fracture surfaces of the failed samples were observed on the FESEM to investigate the causes of failure. Starting with cast samples it was observed that crack initiators were usually porosities since they were the only defect present on the surface, as shown in fig. 5.14 and highlighted by the red circle.

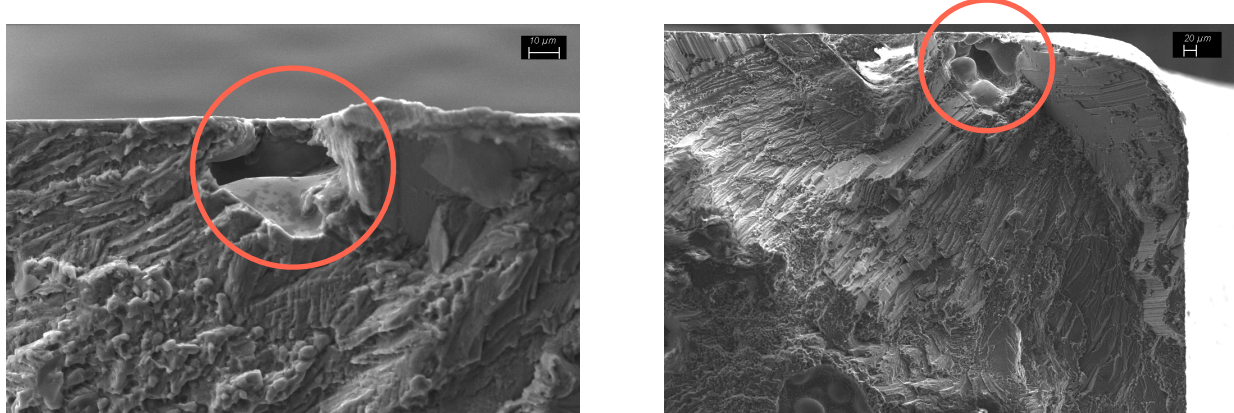
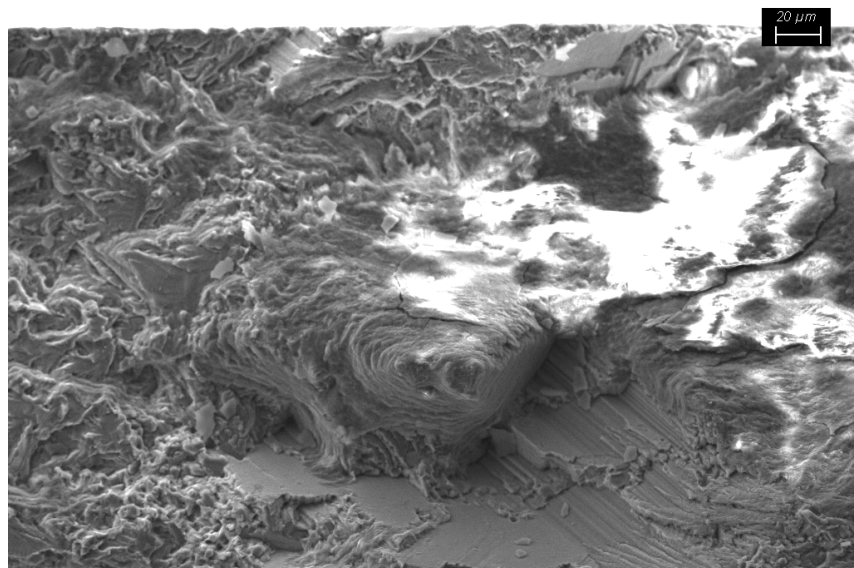
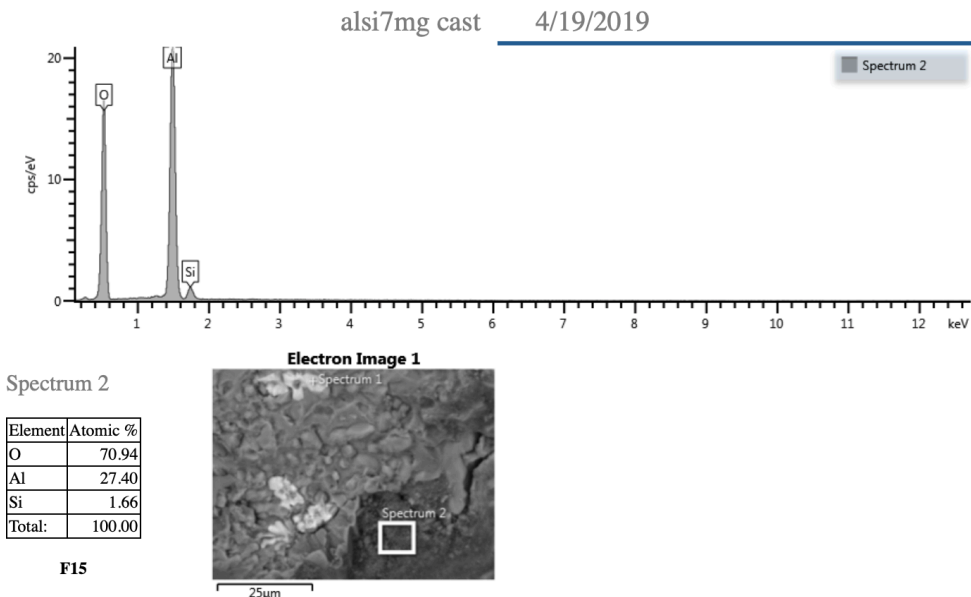


Fig. 5.14 Crack initiation in cast samples

It was found also that brittle oxide inclusions can initiate the crack. The EDS analysis revealed that there were alumina (Al_2O_3) inclusions, probably due to oxidation occurring during the casting process. A typical alumina inclusion is shown in fig. 5.15.



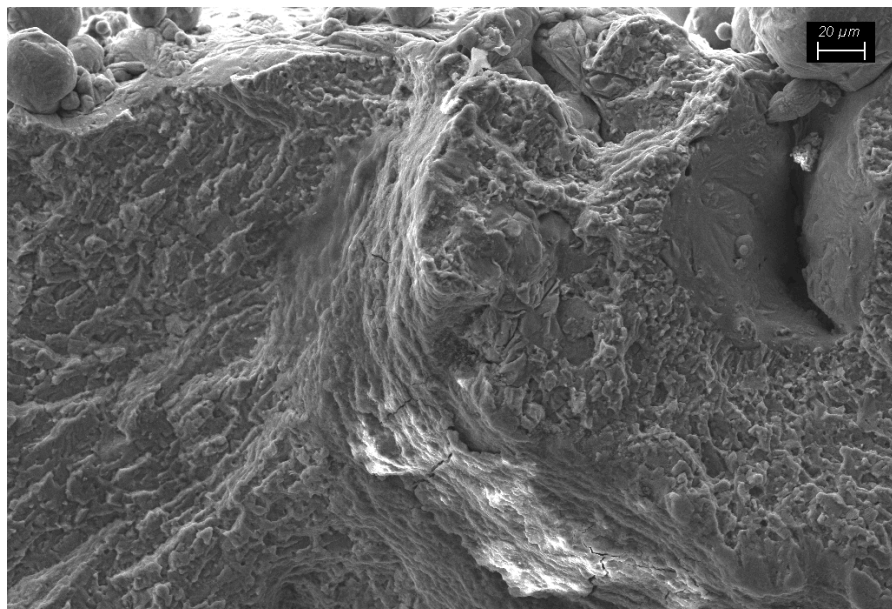
(a)



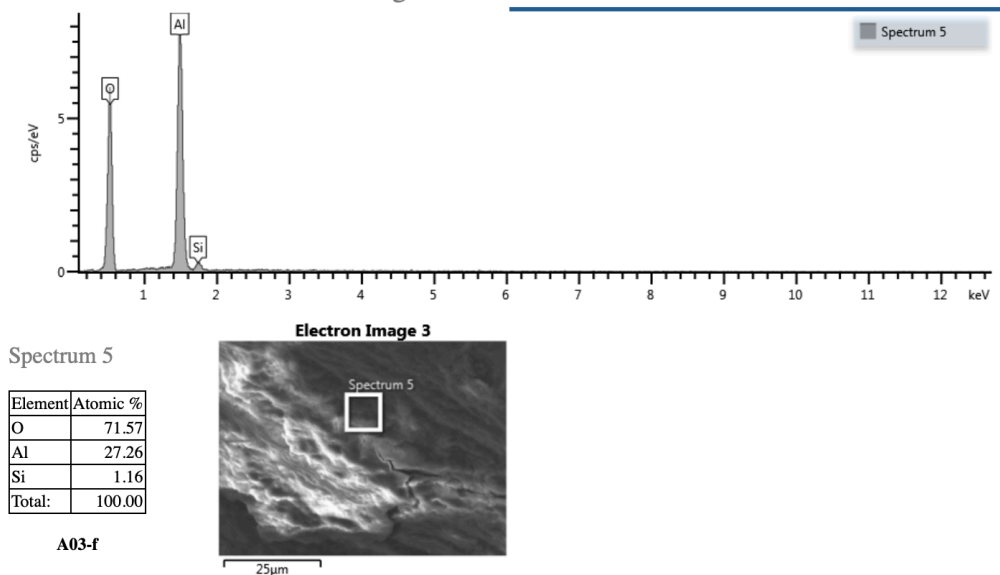
(b)

Fig. 5.15 Alumina surface inclusion on cast sample, (a) SEM micrography, (b) EDS analysis

In fig. 5.15 (a) an inclusion is clearly visible because oxide does not conduct electron and the crust is whiter than the rest of the sample. Similar oxide inclusions were found also in AM samples, and probably due to defects already present in the powders since the SLM process was performed in a controlled atmosphere. This defect is shown in fig. 5.16



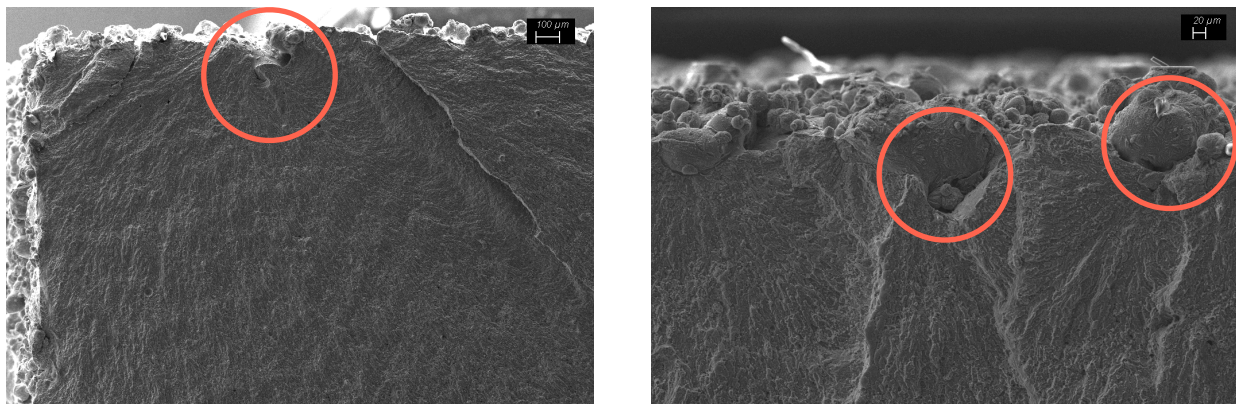
(a)



(b)

Fig. 5.16 Alumina inclusion on fracture surface of AM sample, (a) SEM micrography, (b) EDS analysis

In AM as-built samples frequently, the crack initiators were on the surface, typically porosities or defects due to powders particles only partially sintered on the surface. The initiation points are shown in fig. 5.17(a) porosity and fig. 5.17(b) powders.



(a)

(b)

Fig. 5.17 Crack initiation on AM samples, (a) porosity, (b) powders

Differently, in the tumbled specimens not well sintered particles were removed from the surface so the crack initiators could be inclusions of balled material or porosity. The two types are shown in fig. 5.18.

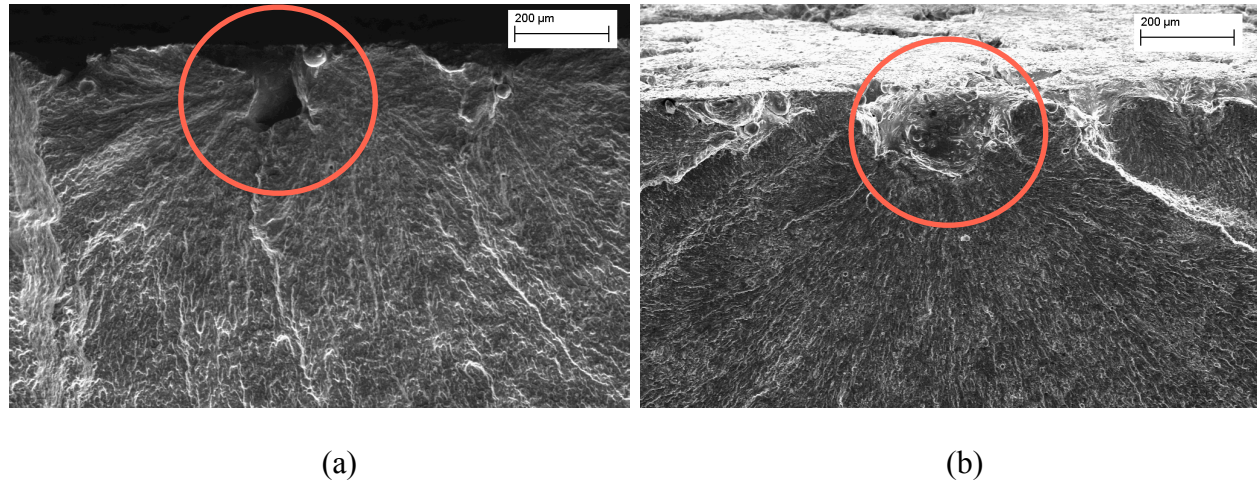
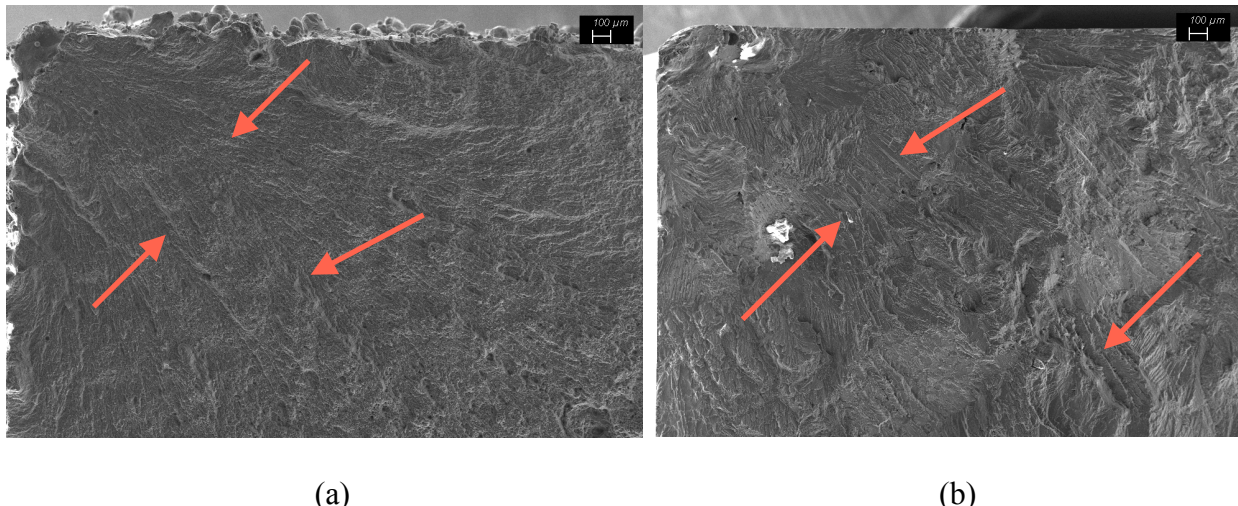
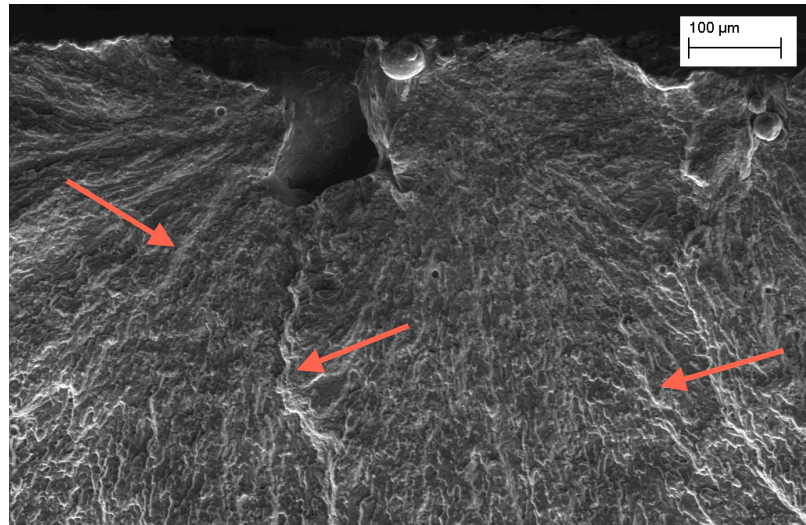


Fig. 5.18 Crack initiation on AM tumbled samples, (a) porosity, (b) inclusion coming from abrasive bodies

The morphology of propagation zone was coarser on the cast samples with respect to the AM ones. The ratchet marks were clearly visible on all specimens, they are shown in fig. 5.19 and highlighted with red arrows. The ratchet marks point directly towards the defect that initiated the crack making it easier to be identified.

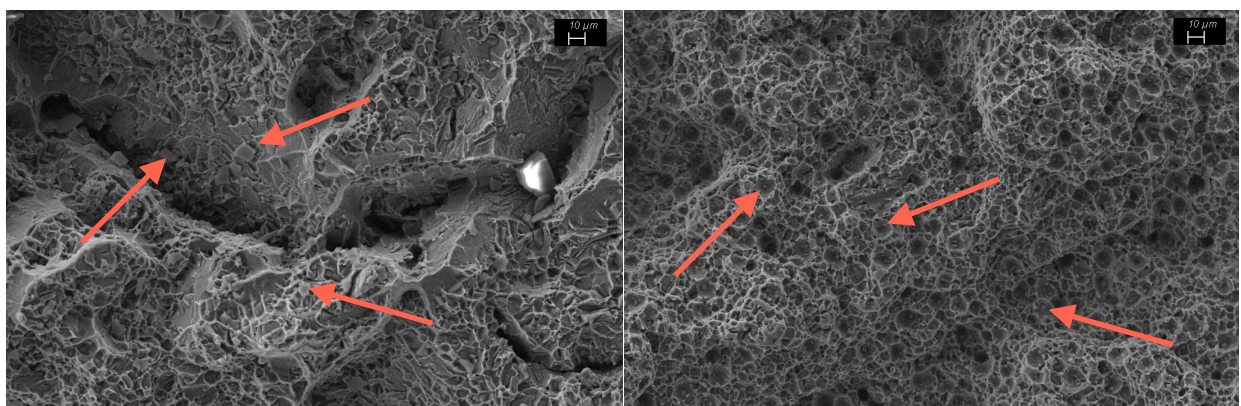




(c)

Fig. 5.19 Propagation zone with ratchet marks (a) AM as-built, (b) AM tumbled and (c) Cast sample

Also the ductile fracture zone was observed. The cast samples presented a semi-ductile fracture with grain decohesion, meaning that there was a component of brittle fracture. Some platelets were found inside the dimples. These platelets are bigger in cast samples while smaller in the AM ones. The EDS analysis revealed that they were silica (SiO_2) platelets, the bigger ones could exert an embrittlement effect. Surface fracture is shown in fig. 5.20 and EDS spectrum in 5.21. The platelets are pointed out with arrows.



(a)

(b)

Fig. 5.20 Ductile fracture (a) cast sample with coarser particles and grain decohesion, (b) AM sample

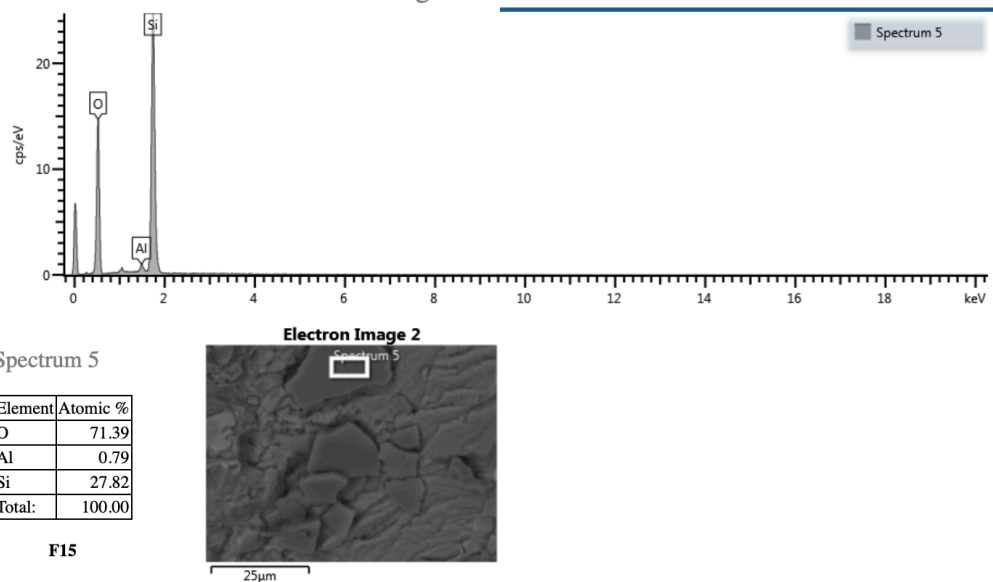


Fig. 5.21 EDS spectrum of silica platelets

5. Conclusions

This work of thesis investigated the fatigue behavior of Al-Si hypoeutectic alloys. The main focus was on the differences between processing paths and surface finishing. The tests performed on the two alloys processed by different processing path allow to draw the following conclusions.

Both from the literature and from our experimental outcomes as well, it is clear that the microstructure of AlSiMg hypoeutectic alloys greatly depends on the processing path:

- Casting gives rise to a rather coarse microstructure with dendritic Al-Si structures at the grain boundaries of Al grains
- Selective laser sintering (SLM) gives rise to a very fine microstructure consisting of mixed Al and Si crystals

After a T6 thermal treatment the microstructure of AlSiMg alloys processed by SLM or by casting becomes very similar, being constituted of:

- Al grains coarsening during the T6 treatment
- Si grains coarsening during the T6 treatment, homogeneously distributed in the case of SLM alloy but concentrated in the dendritic zones of cast alloy
- Needle-like precipitates containing Fe in addition to Al, Si and Mg.
- Very Fine precipitates of Mg_2Si phase, not detectable by optical microscopy.

After the T6 treatment only little differences can be found in the microstructure of SLM and cast AlSiMg alloy:

- The Si crystals are smaller and more homogeneously distributed in the case of SLM samples, while coarser Si grains were placed at the dendritic zones of cast alloys (formerly produced during casting)
- The precipitates containing iron are coarser in the case of cast alloy

Other differences are related to the production path:

- Porosity percentage is similar, but bigger pores can be found in the cast samples
- On the surface of the samples processed by SLM not completely sintered particles can be found, which greatly increases surface roughness
- On the cast samples oxide inclusions can be found

Nevertheless the processing path is different for the two kind of samples (both of them are T6 treated), the mechanical properties such as tensile strength, elastic modulus and hardness) are very similar. However ductility of SLM samples is a bit better.

Three kinds of specimens were submitted to high-frequency flexural fatigue testing:

- T6 treated produced by casting AlSi7Mg alloy with machined surface
- T6 treated produced by SLM AlSi10Mg alloy with very rough surface (as processed)
- T6 treated produced by SLM AlSi10Mg alloy with reduced surface roughness because of tumbling

The fatigue tests was carried out according to a statistic approach (stair case) to obtain the fatigue limit (10^7 cycles). In spite of the worse surface roughness the fatigue limit of SLM samples was better than that of cast samples with very good surface finishing. The fatigue limit of SLM samples further improved after tumbling due to the sharp reduction of the surface roughness.

Examination of the fracture surface showed that crack initiation always occurred at the surface and where are present defects such as:

- Porosity or oxide inclusions mainly in cast samples
- Porosity or not well sintered particles present on the surface of SLM samples
- Porosity or inclusions (coming from the tumbling material) present on the surface of SLM and tumbled specimens

The best fatigue behavior of the SLM samples can be tentatively attributed to the finer microstructure with smaller silicon, precipitate grains and smaller pore size.

6. Bibliography

- [1] Ian Gibson, David Rosen, Brent Stucker, 2015, *Additive Manufacturing Technologies 3D Printing, Rapid Prototyping, and Direct Digital Manufacturing Second Edition*, Springer, New York, USA.
- [2] William D. Callister, Jr, 2001, *Fundamentals of Materials Science and Engineering*, John Wiley & Sons, Inc., USA.
- [3] Li Yang, Keng Hsu, Brian Baughman, Donald Godfrey, Francisco Medina, Mamballykalathil Menon, Soeren Wiener, 2017, *Additive Manufacturing of Metals: The Technology, Materials, Design and Production*, Springer, USA.
- [4] Marco Actis Grande, 2017, *Appunti del corso di Metal Forming Technologies*, Torino
- [5] John O. Milewski, 2017, Additive Manufacturing of Metals, Springer, USA
- [6] C. Y. Yap, C. K. Chua, Z. L. Dong, Z. H. Liu, D. Q. Zhang, L. E. Loh, and S. L. Sing; *Review of selective laser melting: Materials and applications*, Applied Physics Reviews, December 2015
- [7] Mario Rosso, 2017, *Appunti del corso di Ingegneria delle leghe ad elevate prestazioni*, Torino
- [8] P.G. Sheasby and R. Pinner , 2001, *The Surface Treatment and Finishing of Aluminum and Its Alloys, 6th Edition*, ASM international
- [9] S. Otarawanna, A.K. Dahle, *Fundamentals of Aluminium Metallurgy*, 2011
- [10] Michael F. Ashby, David R.H. Jones, *Engineering Materials 2 (Fourth Edition)*, 2013
- [11] Djurdjevic, Mile & Manasijevic, Srecko & Odanović, Zoran & Dolić, Natalija, 2013, *Calculation of Liquidus Temperature for Aluminum and Magnesium Alloys Applying Method of Equivalency*, Advances in Materials Science and Engineering, 2013
- [12] <https://www.cwst.co.uk/services/controlled-shot-peening/>
- [13] S. Zanol, *Efficacia del trattamento di pallinatura sulla resistenza a fatica di leghe d'alluminio*, 2008
- [14] D. Bańkowski, S. Spadło, *Vibratory Machining Effect on the Properties of the Aluminum Alloys Surface*, Archives of Foundry Engineering, 2017
- [15] https://www.efunda.com/formulae/solid_mechanics/fatigue/fatigue_highcycle.cfm
- [16] Collins, Jack A. *Failure of Materials in Mechanical Design Analysis, Prediction, Prevention*. 2nd ed. New York: Wiley, 1993. Print.

- [17] EOS GmbH Electro Optical Systems; "System Data Sheet EOS M 290"
- [18] A. Pantarelli, *Trattamenti termici della lega AlSi10Mg realizzata mediante Additive Manufacturing: microstruttura e proprietà meccaniche*, Torino, 2019
- [19] <https://www.freiberginstruments.com/x-ray-diffraction/technology/theta-scan.html>
- [20] BS EN ISO 6506-1:2014; Metallic materials - Brinell hardness test; Part 1: Test method
- [21] UNI 3964; Prove meccaniche dei materiali metallici, Prove di fatica a temperatura ambiente
- [22] BS EN ISO 6892-1:2016; Metallic materials – Tensile testing; Part 1: Method of test at room temperature
- [23] F. Boiocchi, *Foundry Vs Additive comparison of performances and heat treatments for an Al-Si-Mg alloy*, Metalworking World Magazine, 2019